Journal of *Marine Science and Engineering*

MDPI

Article

Monte Carlo-Based Risk Analysis of Deep-Sea Mining Risers Under Vessel–Riser Coupling Effects

Gang Wang [1,2], Hongshen Zhou [1,2] and Qiong Hu [1,2,*]

[1] School of Mechanical and Electrical Engineering, Central South University, Changsha 410083, China; wgyy529@126.com (G.W.); 233712190@csu.edu.cn (H.Z.)
[2] State Key Laboratory of Deep-Sea Mineral Resources Development and Utilization Technology, Changsha 410012, China
* Correspondence: huqiong@csu.edu.cn; Tel.: +86-18-108470915

Abstract

In deep-sea mining operations, rigid risers operate in a complex and uncertain ocean environment where vessel–riser interactions present significant structural challenges. This study develops a coupled dynamic modeling framework that integrates vessel motions and environmental loads to evaluate the probabilistic risk of riser failure. Using frequency-domain RAOs derived from AQWA and time-domain simulations in OrcaFlex 11.0, we analyze the riser's effective tension, bending moment, and von Mises stress under a range of wave heights, periods, and directions, as well as varying current and wind speeds. A Monte Carlo simulation framework based on Latin hypercube sampling is used to generate 10,000 sea state scenarios. The response distributions are approximated using probability density functions to assess structural reliability, and global sensitivity is evaluated using a Sobol-based approach. Results show that the wave height and period are the primary drivers of riser dynamic response, both with sensitivity indices exceeding 0.7. Transverse wave directions exert stronger dynamic excitation, and the current speed notably affects the bending moment (sensitivity index = 0.111). The proposed methodology unifies a coupled time-domain simulation, environmental uncertainty analysis, and reliability assessment, enabling clear identification of dominant factors and distribution patterns of extreme riser responses. Additionally, the workflow offers practical guidance on key monitoring targets, alarm thresholds, and safe operation to support design and real-time decision-making.

Keywords: deep-sea mining; riser; ocean environment; vessel-riser interaction; probabilistic risk; Monte Carlo simulation; dynamic response; sensitivity

check for updates

Academic Editor: Weicheng Cui

Received: 14 July 2025
Revised: 22 August 2025
Accepted: 28 August 2025
Published: 29 August 2025

Citation: Wang, G.; Zhou, H.; Hu, Q. Monte Carlo-Based Risk Analysis of Deep-Sea Mining Risers Under Vessel–Riser Coupling Effects. *J. Mar. Sci. Eng.* **2025**, *13*, 1663. https://doi.org/10.3390/jmse13091663

Copyright: © 2025 by the authors. Licensee MDPI, Basel, Switzerland. This article is an open access article distributed under the terms and conditions of the Creative Commons Attribution (CC BY) license (https://creativecommons.org/licenses/by/4.0/).

1. Introduction

Deep-sea mining systems are capable of efficiently collecting abundant mineral resources from the seabed and transporting them to surface mining vessels. This not only helps alleviate the growing global demand for critical mineral resources, but also provides high-quality and abundant metallic and non-metallic mineral resources for human use [1]. The currently explored seabed resources include cobalt-rich ferromanganese crusts, as well as a variety of potentially exploitable polymetallic nodules and polymetallic sulfides [2,3]. Many countries have conducted relevant theoretical studies and offshore experiments on mineral extraction.

At present, most deep-sea mining systems adopt hydraulic pipeline lifting systems, in which the surface mining vessel is connected to the seafloor mining vehicle via a vertical

riser and a lifting pump [4]. After the mining vehicle collects and crushes seabed materials, the resulting sand and slurry are transported to the surface vessel through flexible hoses, intermediate buffer chambers, and the riser pipe, driven by the lifting pump [5–7]. Among these components, the lifting system serves as the key conduit connecting the seafloor mining equipment to the surface vessel, and its structural integrity and dynamic response characteristics are directly related to the continuity of mining operations, the overall stability of the system, and deep-sea ecosystem security [8,9]. In particular, under complex and variable uncertain ocean environments, significant fluid–structure interaction occurs between the mining vessel and the riser system [10]. The vessel undergoes multi-degree-of-freedom motions induced by ocean environmental loads such as waves, currents, and winds. These motions are transmitted to the riser through hangers and connectors, leading to time-varying dynamic structural responses including bending moments, axial tension, and fatigue accumulation.

Numerous studies have been conducted on the dynamic characteristics of the mining riser under the coupling effect between the mining vessel and the riser system. Song et al. [11] developed an indirect time-domain coupled dynamic model for the mining vessel and riser system. Through simulation and experimental validation, they evaluated the effects of regular waves, intermediate buffer mass, and vessel speed on the vessel–riser coupling dynamics. They demonstrated that the coupling effect significantly influences the dynamic behavior of both the vessel and the riser. Chen et al. [12] investigated the dynamic response and spatial position variations of the riser system under different cooperative velocities and directions of the mining vessel and vehicle. Their experimental results further confirmed that the dynamic characteristics of the riser system are strongly affected by the coupled motion of the surface vessel and the seabed mining vehicle. Wu et al. [13], using a lumped mass approach, calculated the hydrodynamic forces induced by waves and the impact of vessel motion in irregular wave conditions on the dynamics of the riser system. Their results also identified wave-induced vessel motion as a critical driver of riser system response. Zhu et al. [14] developed a coupled model incorporating the mining vessel, riser system, and lifting pump, which also accounted for dynamic positioning and active heave compensation of the vessel. Using a neural network–based approach, they predicted the dynamic responses of pump motion and riser tension, demonstrating that wave frequency motions exert a significant influence on the dynamic behavior of the seabed mining system. Similarly, Li et al. [15] investigated the axial force variations and parametric vibrations of the deep-sea mining riser under the heave motions of the mining vessel. In addition, several studies have employed numerical simulations to investigate the coupled dynamics between floating structures and auxiliary equipment such as marine risers under wave action [16–19]. These existing studies have, to some extent, revealed the coupling mechanisms between vessels and risers under wave loading and their significant impact on system dynamics, emphasizing the need to ensure that the riser operates within safe limits in practical engineering applications.

Sun et al. [20] demonstrated that under the influence of internal solitary waves, an installed deep-sea mining system can experience large-scale displacements, significantly increasing the risk of collision with other subsea equipment. This finding highlights the necessity of emphasizing the failure risks of the deep-sea riser system to ensure the safe implementation of mining operations. With regard to the performance and structural safety of rigid mining risers, existing studies have primarily focused on investigating their dynamic responses under complex ocean environmental conditions. Hu et al. [21] established a numerical simulation model to conduct both static and dynamic analyses of the flexible hose. Based on key monitoring points identified in the analysis, they developed a neural network model to predict the dynamic response of the pipe, enabling early

performance monitoring under complex ocean conditions. In a more comprehensive parameter sensitivity study, Cao et al. [22] proposed a three-dimensional numerical model of the entire mining system based on the intrinsic finite element (VFIFE) method. They analyzed the influence of vessel motion, internal and external pipe flows, and buffer mass on the riser dynamics. Xiao et al. [23] conducted numerical simulations to investigate the strength and hydrodynamic responses of flexible risers in a deep-sea mining system under coupled operations. They proposed a coordinated motion control strategy between two moored subsea devices, providing a safe and effective solution for mining control systems. Regarding the longitudinal vibration of mining risers, Liu et al. [24] analyzed the vibration characteristics of a 5000 m riser under various wind conditions, offset angles, damping ratios, and ore hold weights. Moreover, given the considerable length of mining risers, which can extend several kilometers, current-induced vibrations of different modal responses are likely to occur, while vortex-induced vibrations (VIVs) can lead to fatigue damage. To ensure the safe operation of deep-sea mining systems, several studies have focused on the vibration characteristics of risers under transverse current loading [25–28] and the fatigue effects of vortex-induced vibrations on mining risers [29,30]. Lin et al. [31] also investigated the VIVs of marine risers under non-uniform current loading. Using a CFD–FEM bidirectional fluid–structure interaction approach, they identified that the riser's most vulnerable region lies in the upper one-third of its length. When the excitation frequency of VIV approaches the natural frequency of the marine riser, resonance may occur. Building on this issue, Wang et al. [32] analyzed the natural frequencies of deep-sea mining risers under different tension conditions and the presence of buffer stations. To further mitigate VIVs, Deng et al. [33] proposed a control strategy that combines the Iwan–Blevins wake oscillator model with Morison-based hydrodynamic analysis. Specifically, they demonstrated that adjusting the internal fluid density and buffer mass can effectively modify vibration amplitudes. The safety of riser vibrations must consider not only the influence of external currents but also the internal flow of mineral slurry. Dai et al. [34] and Duan et al. [35] developed multibody dynamic models that simultaneously account for internal and external flows, providing insights for pipeline design and performance evaluation. In addition to the normal mining operation phase, Wang et al. [36] analyzed the deployment process of deep-sea mining risers under the influence of internal solitary waves, focusing on the riser configuration, tension, stress, upper-end rotation, offset, and transient responses. Their study identified the critical stages and key risk factors during deployment. In related offshore engineering applications such as oil and gas exploitation, Gu et al. [37] considered wake interference effects, and based on the VFIFE method developed a dual-riser model to predict the probability of riser collision. Similarly, Mao et al. [38] incorporated the coupled effects of external ocean currents and internal multiphase flows to establish a VIV response model for production risers, thereby improving the operational safety of riser systems in offshore oil and gas production.

Risk assessments require both qualitative understanding and quantitative estimations of failure probability. Some studies have applied methods such as the analytic hierarchy process (AHP), fault tree analysis (FTA), and Bayesian fault analysis for reliability assessments and identification of key risk factors in other offshore pipeline structures [39–42]. In the context of deep-sea mining, Ma et al. [43] applied an AHP to conduct a comprehensive risk assessment of mineral extraction activities, covering political, economic, engineering, and environmental aspects. However, their work did not focus on the structural risks of mining equipment. Lu et al. [44] developed a traversability evaluation model based on AHP and fuzzy comprehensive evaluations to assess the operational performance of mining vehicles and enhance the identification of hazardous seabed areas. Nevertheless, these approaches lack probabilistic modeling and analyses of stochastic environmental

disturbances on deep-sea mining pipeline systems. Moreover, the AHP is inherently subjective, relying heavily on expert judgment and weight assignments, which can introduce bias into the results.

To provide a comprehensive summary and critical analysis of existing studies, Table 1 presents a selection of representative papers along with their main research focus and limitations.

Table 1. Research contents and limitations of related studies.

Authors and Year	Main Contributions	Limitations
Song et al. (2022) [11]	Evaluation of the effects of regular waves, intermediate hold mass, and sailing speed on vessel–riser coupled dynamics	Inadequate consideration of uncertainties in complex ocean conditions
Chen et al. (2021) [12]	Dynamic response of the lifting system under different coordination modes between the mining vessel and the seafloor miner	Insufficient development of probabilistic risk modeling and quantitative evaluation; inadequate consideration of uncertainties in complex ocean conditions
Wu et al. (2021) [13]	Influence of wave-induced hydrodynamic loads and vessel motions under irregular waves on the dynamics of deep-sea mining lifting systems	A limited sensitivity analysis and incomplete treatment of parameter uncertainties; inadequate consideration of uncertainties in complex ocean conditions
Li et al. (2025) [15]	Variation of axial force and parametric vibration analysis of the deep-sea mining riser subjected to heave motions of the mining vessel	A limited sensitivity analysis and incomplete treatment of parameter uncertainties; inadequate consideration of uncertainties in complex ocean conditions
Sun et al. (2022) [20]	Impact of internal solitary waves on deep-sea mining operations	Insufficient investigation of vessel–riser multi-factor coupling; a limited sensitivity analysis and incomplete treatment of parameter uncertainties; inadequate consideration of uncertainties in complex ocean conditions
Hu et al. (2024) [21]	Development of a neural-network-based predictive model for riser dynamic responses in deep-sea mining	Insufficient investigation of vessel–riser multi-factor coupling; inadequate consideration of uncertainties in complex ocean conditions
Cao et al. (2023) [22]	Modeling and dynamic analysis of the integrated vertical transport system for deep-sea mining based on VFIFE	A limited sensitivity analysis and incomplete treatment of parameter uncertainties; inadequate consideration of uncertainties in complex ocean conditions
Deng et al. (2025) [33]	Adjustment of nonlinear riser tension using a wake oscillator model combined with Morison's equation for VIV control strategy	Inadequate consideration of uncertainties in complex ocean conditions
Cheliyan, A.S. (2018) [40]	A fuzzy fault tree analysis of oil and gas leakage in subsea production systems	Lack of objective and statistically significant tools for risk assessment
Zhang et al. (2019) [42]	Construction of a risk assessment framework for oil and gas pipelines based on a quantitative risk analysis	Lack of objective and statistically significant tools for risk assessment

Based on the results summarized in Table 1, it can be seen that significant progress has been achieved in the areas of dynamic modeling and response analyses of deep-sea mining risers, ship–riser coupled dynamics, and safety assessments and control of dynamic responses. However, several gaps remain. First, the systematic consideration of uncertainties

in complex ocean environments is still insufficient. Many studies fail to fully capture the stochastic influences of waves, currents, winds, and their interactions on the dynamic response of rigid risers. Second, despite the fact that riser dynamics are subject to multi-factor interactions, probabilistic risk modeling and quantitative assessments remain underdeveloped, and a comprehensive probability-based framework for failure risk evaluation has not yet been established. Third, the lack of large-sample, multi-parameter sensitivity analyses make it difficult to identify the key risk factors governing riser safety. Moreover, studies on fully coupled ship–riser–current interactions are still limited. In addition, traditional risk assessment approaches used in related marine engineering equipment, such as the AHP and fault tree analyses, rely heavily on expert judgment and subjectively assigned weights, which limit their objectivity and statistical rigor. Consequently, there is still a lack of integrated methodologies capable of simultaneously analyzing riser dynamics and quantifying probabilistic risks under complex ocean conditions. Such methodologies are critical to ensuring that the operational safety of deep-sea mining risers remains within acceptable limits under random environmental disturbances.

The scientific problem addressed in this study is how to develop a dynamic model that accurately captures multi-factor ship–riser coupling under complex, uncertain ocean conditions, and on that basis to quantify failure risk and assess the reliability of rigid mining risers. Compared with qualitative risk assessment methods like AHP, Monte Carlo simulations offer greater numerical modeling capability and objective statistical significance without requiring complex evaluations [45]. This approach has been increasingly applied in engineering practices for structural risk analyses [46–48]. Therefore, this study proposes introducing a Monte Carlo simulation into the risk assessment of the mining riser under vessel–riser coupled conditions. The objective is to establish a risk modeling approach for riser dynamic responses in uncertain ocean environments, integrating a frequency-domain hydrodynamic response analysis, vessel–riser dynamic coupling simulations, a Monte Carlo-based reliability assessment, and a sensitivity analysis. This framework aims to provide a robust technical foundation for future structural safety evaluations and layout optimization of deep-sea mining pipelines. To achieve this objective, a high-fidelity mining vessel model was first established in ANSYS AQWA 2024 R2, and a hydrodynamic analysis was performed to obtain the six-degree-of-freedom response amplitude operators (RAOs). These RAOs were then imported into OrcaFlex as boundary conditions to develop a coupled vessel–riser dynamic model of the deep-sea mining system [49]. A large number of stochastic sea state samples were generated using Latin hypercube sampling, and a probabilistic risk model of the rigid riser dynamic response was constructed based on the Monte Carlo method to quantify failure probability and system reliability. Subsequently, a multi-parameter Sobol sensitivity analysis was conducted to identify the environmental risk factors with the greatest influence on riser safety. Finally, operational guidelines for the safe performance of rigid risers in complex environments were proposed, providing a theoretical foundation for structural design optimization, real-time monitoring, and risk-informed decision making. Beyond theoretical contributions, these insights hold substantial practical significance in translating the findings into actionable engineering guidelines.

2. Methods and Theories

2.1. Modeling Assumptions

In practical engineering applications, a deep-sea mining riser system typically consists of a rigid lifting pipe, flexible hose, lifting pump, and intermediate buffer. The dynamic response of the system is significantly influenced by complex factors such as marine environmental conditions, installation constraints, and coupled interactions among components. To

enable efficient modeling of the deep-sea mining system and achieve accurate vessel–riser coupled numerical simulations, the following simplifying assumptions are made:

(1) The vessel is modeled as a rigid body, and its structural elasticity and deformations are neglected. Its responses under wave excitation are described by the response amplitude operators (RAOs) obtained through a linear frequency-domain hydrodynamic analysis;
(2) Environmental loads are assumed to be linearly superimposed. The wave field is generated using a linear superposition of random waves. The current direction is assumed to lie in the same plane as the riser deformation, with a power law profile along the depth;
(3) Nonlinear contact mechanics between the riser and components, such as the intermediate buffer and lifting pump, are neglected. The bottom boundary of the riser is modeled as either fixed or simply supported, and the force contribution from the flexible hose to the buffer is ignored;
(4) Structural damping is represented using an equivalent linear damping model, while nonlinear friction, fatigue, and impact effects are not considered;
(5) The riser is modeled as a continuous pipe with uniform material properties and isotropy in the mechanical analysis;
(6) The internal details of the intermediate buffer and lifting pump are neglected, and they are idealized as mass points with lumped mass properties;
(7) Hydrostatic pressure and buoyancy are reflected in the effective tension distribution along the riser;
(8) Material properties are assumed pressure-insensitive within the elastic range, while potential hydrostatic collapse or local buckling effects are beyond the present scope.

2.2. Dynamic Analysis of the Vessel–Riser Coupled Model

Significant dynamic coupling exists between the mining vessel and the rigid riser in a deep-sea mining system. Under the combined excitation of wind, waves, and currents, the vessel undergoes six degrees of freedom (6-DOF) motions. These motions are transmitted to the riser system through the top connection point, inducing tension fluctuations and lateral vibrations along the riser. Meanwhile, due to the riser's inherent flexibility and large deflection characteristics, it exerts reactive forces on the vessel, affecting its attitude and dynamic response. This bidirectional coupling fundamentally determines the overall force distribution and operational safety of the system. The coupled interaction can be simplified as a floating body–riser system, the dynamic behavior of which must account for top boundary disturbances caused by the vessel's 6-DOF motion, the riser's axial tension and bending responses, and hydrodynamic excitation from currents and wave loading. A schematic of the vessel–riser coupling system for deep-sea mining is illustrated in Figure 1.

Based on the assumptions outlined in Section 2.1, the rigid riser can be simplified as a tensioned elastic Euler–Bernoulli beam during modeling. Its transverse dynamic response under wave–current excitation and vessel-induced disturbances is considered. Assuming the riser is vertically oriented, and letting its horizontal transverse displacement be denoted as $\omega(z,t)$, the governing dynamic equation is given by:

$$EI\frac{\partial^4\omega(z,t)}{\partial z^4} - \frac{\partial}{\partial z}\left(T(z)\frac{\partial\omega}{\partial z}\right) + m\frac{\partial^2\omega(z,t)}{\partial t^2} + c\frac{\partial\omega(z,t)}{\partial t} = f(z,t) \quad (1)$$

where EI is the bending stiffness of the riser (the product of Young's modulus and the second moment of area); $T(z)$ is the tension distribution along the vertical axis; m is the mass per unit length; c is the linear structural damping coefficient; $f(z,t)$ represents external

excitations including wave loading, hydrodynamic drag, and vessel-induced disturbances; $\omega(z,t)$ is the transverse displacement function of the riser.

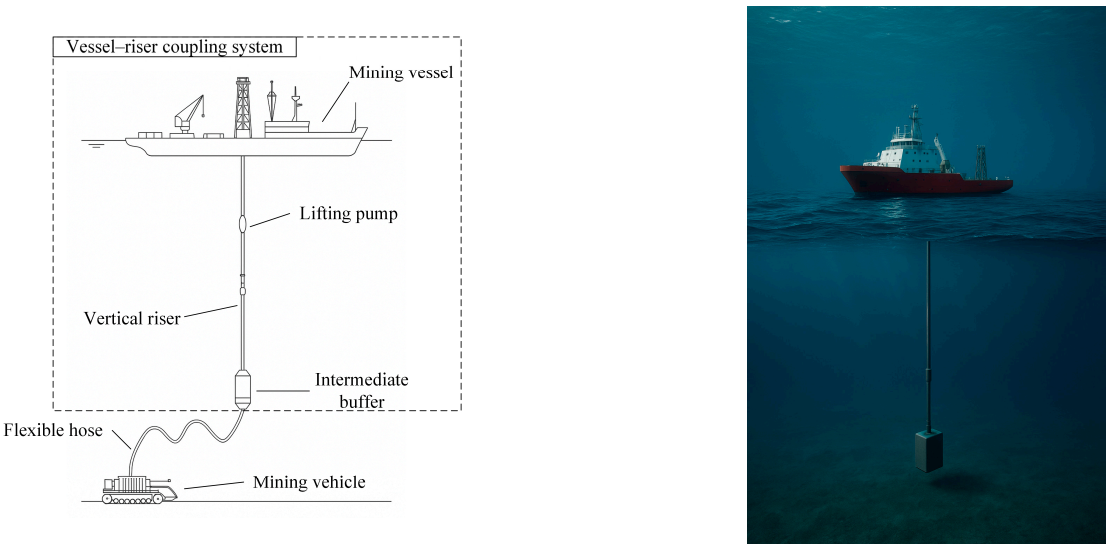


Figure 1. The schematic of the vessel–riser coupling system for deep-sea mining: (**a**) schematic diagram of the deep-sea mining system; (**b**) 3D model of the vessel–riser coupling system.

The tension term $T(z)$ can be computed using the following integral expression:

$$T(z) = T_{top} - \int_0^z mgdz = T_{top} - mgz \tag{2}$$

Here, T_{top} denotes the applied tension at the riser top, and g is the gravitational acceleration.

In the boundary condition setup, the top end of the riser is connected to the mining vessel via a gimbal mechanism, allowing it to follow the vessel's six degrees of freedom motion.

$$\omega(0,t) = \omega_s(t), \frac{\partial \omega}{\partial t}(0,t) = \theta_s(t) \tag{3}$$

The displacement disturbance caused by vessel heave is denoted by $\omega_s(t)$, while $\theta_s(t)$ represents the rotational boundary condition induced by pitch or roll motions.

The lower end of the riser is modeled as a free end, connected to a flexible hose via an intermediate buffer. The flexible hose is fixed at both ends—connected to the buffer and to the seabed mining vehicle. Buoyancy modules are arranged along the hose to form an arch-like configuration.

Under this configuration, the mining vessel and the riser can be regarded as two coupled vibrating subsystems. Let $X_s(t)$ represent the vessel displacement in its principal motion direction and $X_p(t)$ denote the key structural response of the riser. The governing equations for the coupled system are then expressed as:

$$\begin{cases} M_s\ddot{X}_s + C_s\dot{X}_s + K_sX_s + K_{sp}(X_s - X_p) = F_{wave}(t) \\ M_p\ddot{X}_p + C_p\dot{X}_p + K_pX_p + K_{ps}(X_p - X_s) = F_{pipe}(t) \end{cases} \tag{4}$$

where M_s and M_p are the effective masses of the vessel and the riser, respectively; C_s and C_p are the damping coefficients; K_s and K_p are the stiffness coefficients; K_{sp} and K_{ps} are the coupling stiffness terms; $F_{wave}(t)$ and $F_{pipe}(t)$ represent the wave excitation force and hydrodynamic force acting on the pipe, respectively.

2.3. Vessel RAO Theory

The response amplitude operator (RAO) is a fundamental hydrodynamic parameter used to characterize the frequency response behavior of floating structures under regular wave excitation. It quantifies the ratio between the amplitude of the structural response in a specific degree of freedom and the amplitude of the incident wave at a given wave frequency. For any motion direction iii in the six degrees of freedom (6-DOF) of a floating structure, the RAO is defined as:

$$RAO_i(\omega) = \frac{X_i(\omega)}{\gamma(\omega)} \tag{5}$$

where $RAO_i(\omega)$ is the response amplitude operator in the i-th degree of freedom, $X_i(\omega)$ is the motion amplitude of the structure in that direction, $\gamma(\omega)$ is the incident wave amplitude, and $\omega = 2\pi/T$ is the wave angular frequency.

According to potential flow theory and under the assumption of small-amplitude motion, the velocity potential $\varnothing$ in the flow field can be decomposed using the principle of superposition into three components:

$$\varnothing = \varnothing_I + \varnothing_R + \varnothing_D \tag{6}$$

where $\varnothing_I$ is the incident potential, representing the velocity potential of pure waves in the absence of a structure; $\varnothing_R$ is the radiation potential, representing the potential field induced by forced oscillations of the structure in the absence of incident waves; $\varnothing_D$ is the diffraction potential, accounting for the wave–structure interaction when the structure is fixed.

The complete velocity potential acting on the vessel can be obtained by solving the boundary value problems for each of the three components. The incident potential $\varnothing_I$ can be derived analytically using linear wave theory. However, due to the nonlinear boundary conditions involved in $\varnothing_R$ and $\varnothing_D$, these potentials are typically solved using numerical discretization methods.

Assuming only wave loads are considered and the vessel undergoes motion, the time-domain motion equation can be written as:

$$M_{kj}\zeta_j(t) = f_j^W(t) - C_{kj}\zeta_j(t) \tag{7}$$

where $f_j^W(t)$ is the wave excitation force, obtained by integrating the fluid pressure over the body surface, and $C_{kj}\zeta_j(t)$ represents the hydrostatic restoring force.

Applying a Fourier transform to the time-domain equation yields the frequency-domain form:

$$-\omega^2 M_{kj}X_j(\omega) + C_{kj}X_j(\omega) = F_j^W(\omega) \tag{8}$$

The wave excitation force due to incident and diffraction potentials can be expressed as:

$$F_j^{exc}(\omega) = -i\omega\rho\iint(\varnothing_I + \varnothing_D)n_j dS \tag{9}$$

Assuming a wave force $G_j(\omega, \beta)$ is generated by a unit wave amplitude from an incident direction, then for an actual wave amplitude ζ_a, the excitation force becomes:

$$F_j^{exc}(\omega, \beta) = \zeta_a G_j(\omega, \beta) \tag{10}$$

The radiation force component can be written as:

$$F_j^{eR}(\omega) = \omega^2 A_{kj}(\omega)X_j(\omega) - i\omega B_{kj}(\omega)X_j(\omega) \tag{11}$$

where $A_{kj}(\omega)$ is the added mass term and $B_{kj}(\omega)$ is the potential damping term.

Substituting Equations (9) and (10) into Equation (7), the final expression becomes:

$$-\omega^2\left[M_{kj}+A_{kj}(\omega)\right]X_j(\omega)+i\omega B_{kj}(\omega)X_j(\omega)+C_{kj}X_j(\omega)=\zeta_a G_j(\omega,\beta) \tag{12}$$

Defining $H_j(\omega,\beta)$ as the motion response amplitude induced by a unit wave height in direction β, the final expression becomes:

$$H_j(\omega,\beta)=\left[-\omega^2\left(M_{kj}+A_{kj}(\omega)\right)+i\omega B_{kj}(\omega)X_j(\omega)+C_{kj}\right]^{-1}G_j(\omega,\beta) \tag{13}$$

where $H_j(\omega,\beta)$ represents the motion amplitude response operator (RAO) of the vessel. This formulation can be solved separately for each degree of freedom to obtain the corresponding RAOs.

2.4. Wind–Wave–Current Load Theory

2.4.1. Wind Load

The wind load primarily affects the surface mining vessel, while the influence on the underwater transport and operation system is relatively limited. However, due to the integrated nature of the deep-sea mining system, the vessel's motion is strongly coupled with the behavior of the underwater equipment. The wind force and moment acting on the vessel can be calculated using the following equations:

$$\begin{cases} F_{xw}=0.5C_{xw}\rho_w V_w^2 A_T \\ F_{yw}=0.5C_{yw}\rho_w V_w^2 A_L \\ M_{xyw}=0.5C_{xyw}\rho_w V_w^2 A_L L_{BP}^2 \end{cases} \tag{14}$$

where F_{xw} and F_{yw} denote the wind load acting in the longitudinal and transverse directions of the vessel, respectively; M_{xyw} is the wind load moment acting on the vessel's direction; C_{xw}, C_{yw}, and C_{xyw} are the wind force coefficients in each respective direction; ρ_w is the air density; v_w is the mean wind speed; A_T and A_L are the projected wind areas of the vessel above the waterline in the transverse and longitudinal directions, respectively; L_{BP} is the length between perpendiculars of the vessel.

2.4.2. Current Load

Currents exert hydrodynamic forces on the entire deep-sea mining system. Strong currents may cause significant increases in structural stress. The forces induced by currents are typically evaluated using well-established engineering formulations. The current loads on the mining vessel and flexible risers can be estimated as follows:

$$\begin{cases} F_{xc}=0.5C_{xc}\rho_c V_c^2 T L_{BP} \\ F_{yc}=0.5C_{yc}\rho_c V_c^2 T L_{BP} \\ M_{xyc}=0.5C_{xyc}\rho_c V_c^2 T L_{BP}^2 \end{cases} \tag{15}$$

where F_{xc}, F_{yc}, and M_{xyc} are the current force components and moment acting on the vessel; C_{xc}, C_{yc}, and C_{xyc} are the drag coefficients in each respective direction; ρ_c is the seawater density; V_c is the mean current speed; T is the draft of the mining vessel.

The current-induced force on the flexible riser is calculated as:

$$F_c=\frac{1}{2}C_d\rho_c A u_c^2 \tag{16}$$

where F_c is the current force acting on the flexible riser; C_d is the drag coefficient; A is the projected area of the riser in the current direction; u_c is the current speed.

2.4.3. JONSWAP Spectrum Theory and Wave Load Calculation

Ocean waves are inherently irregular and can be treated as a stationary stochastic process. Their dynamic behavior can be simulated by linearly superposing multiple regular waves. The relationship among the wave energy, frequency, and direction can be characterized by a wave spectrum. In this study, the JONSWAP spectrum is employed, where the irregular sea state is considered as a superposition of regular waves with varying amplitudes, frequencies, and phases. The spectral density function is given by:

$$S(f) = \left(\frac{\alpha g^2}{16\pi^4}\right) f^{-5} exp\left[\frac{-5}{4}\left(\frac{f}{f_m}\right)^{-4}\right] \gamma^{exp[\frac{-1}{2\sigma^2(f/fm-1)^2}]} \tag{17}$$

In the equation, the definition of α is as follows:

$$\alpha = \frac{0.0624}{0.230 + 0.0336\gamma - 0.185(1.9+\gamma)^{-1}} \tag{18}$$

In the equation, $S(f)$ represents the wave spectrum; α is a dimensionless coefficient related to the significant wave height H_s and the zero-crossing wave period T_z; γ is the peak enhancement factor; f denotes the wave frequency; f_m is the peak frequency; σ is the spectral width parameter.

The relationship between the amplitude of the j-th regular wave component and the wave spectrum and the expression for calculating the time history ψ of the varying significant wave heights are given as follows:

$$\frac{1}{2}A_j^2 = S(f_j)\Delta\omega \tag{19}$$

In the equation, A_j is the wave amplitude and ω is the angular frequency.

$$\psi = \sum_{j=1}^{N} A_j sin(\omega_j t - k_j x + \epsilon_j) \tag{20}$$

In the equation, N is the number of superimposed regular wave components, k_j is the wave number, and $\grave{o}_j$ is the random phase, which is in the range of $(0, 2\pi)$.

Wave loads on deep-sea mining risers are calculated using a combination of wave theory and a wave spectrum analysis. Given the large slenderness ratio of risers, the Morison equation—a semi-empirical approach—is typically used for wave force estimation. The classical Morison equation assumes the structure to be rigid and fixed at the seabed. For large lateral motions or for floating or flexible risers, the structural orientation changes and the water particle velocities or accelerations are no longer aligned with the riser axis. Therefore, a vector formulation of velocity must be used.

The differential form of the Morison equation is:

$$dF = C_M \rho dV \dot{\mu}_n + \frac{1}{2} C_D \rho dA |\mu_n| \mu_n \tag{21}$$

In the equation, dF is the elemental wave force; dV and dA are the volume and projected area of the riser segment, respectively; C_M is the inertia coefficient; C_D is the drag coefficient; μ_n and $\dot{\mu}_n$ are the velocity and acceleration of the fluid particle normal to the riser axis, respectively; ρ is the seawater density.

After integration, the total wave force can be expressed as:

$$F = \rho \frac{\pi D^2}{4} \dot{\mu}_n C_M + \frac{\rho D}{2} |\mu_n| \mu_n C_D \tag{22}$$

In the equation, D is the riser diameter. The total wave load F is the sum of the inertial force due to fluid acceleration and the viscous drag force.

2.5. Theory of Monte Carlo Simulation and Sensitivity Analysis

Under complex marine environmental conditions, the dynamic response of deep-sea mining risers exhibits a high degree of uncertainty. The coupled effects of environmental loads lead to strongly nonlinear and sensitive responses in the riser structure. Traditional deterministic approaches are insufficient to comprehensively assess the risk of extreme structural responses; thus, it is necessary to introduce risk assessment techniques grounded in probabilistic and statistical methods.

The Monte Carlo method is a numerical integration technique that estimates the statistical distribution of a system's output by sampling a large number of random inputs that span the entire input space of a complex system. Let the input to the structural system be represented by an n-dimensional random vector $X = [X_1, X_2, \ldots, X_n]^T$ and the system response be defined by the function $Y = g(X)$. If a failure criterion is defined as $g(X) > y_{lim}$, then the probability of failure can be estimated as:

$$P_f = \iint_{\Omega_f} f_X(x)dx \approx \frac{1}{N}\sum_{i=1}^{N} I[g(X) > y_{lim}] \tag{23}$$

In the equation, $f_X(x)$ is the joint probability density function (PDF) of the input vector; N is the total number of simulation samples; I is the indicator function, which equals 1 if the condition is met and 0 otherwise.

To identify the most influential uncertain parameters, this study adopts the Sobol sensitivity indices based on variance decomposition. Assuming the total output response is $Y = g(X)$, the variance of the output can be decomposed into contributions from each input and their interactions:

$$Var(Y) = \sum_{i=1}^{n} V_i + \sum_{i<j} V_{ij} + \ldots + V_{1,2,\ldots,n} \tag{24}$$

where V_i represents the first-order effect of the i-th input variable.

The first-order Sobol index is defined as:

$$S_i = \frac{V_i}{Var(Y)} \tag{25}$$

The total Sobol index, which accounts for both the first-order and higher-order effects of the i-th input, is defined as:

$$S_{T_i} = 1 - \frac{Var_{\sim X_i}\left[E_{X_i}[Y|\sim X_i]\right]}{Var(Y)} \tag{26}$$

where $\sim X_i$ denotes all variables except X_i.

By estimating the Sobol indices, the influence of each input variable on the uncertainty of the system output can be quantified. A higher index value indicates a greater contribution to output variability.

3. Risk Analysis Framework for Mining Risers Based on Monte Carlo Simulation

The overall risk analysis workflow for the deep-sea mining riser system under vessel–riser coupling conditions is illustrated in Figure 2.

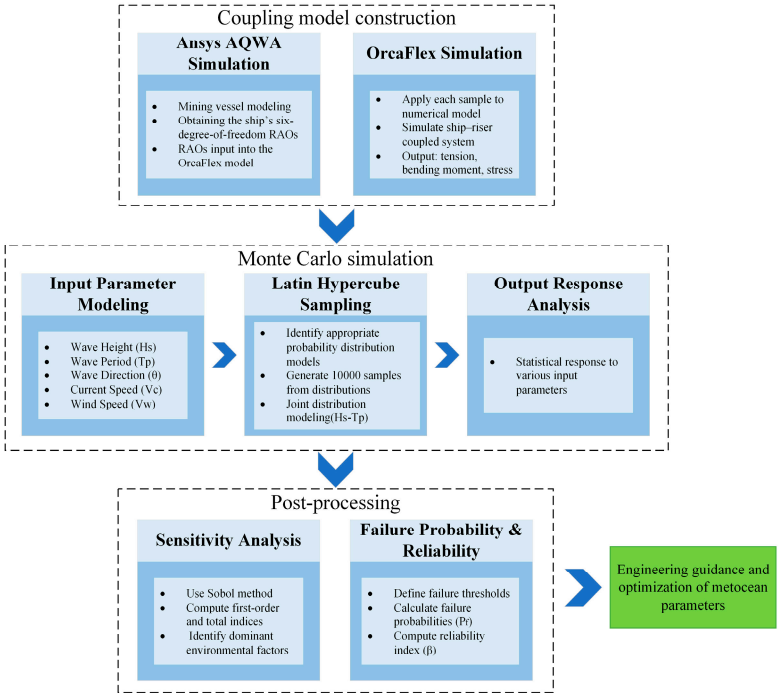


Figure 2. The overall risk analysis workflow for the deep-sea mining riser system under vessel–riser coupling conditions.

The overall analysis procedure begins with the development of a hydrodynamic model of the deep-sea mining vessel in AQWA, where the six-degree-of-freedom RAOs are obtained and subsequently imported into the OrcaFlex simulation model to construct a coupled vessel–riser system. For the Monte Carlo simulation, input models of ocean environmental parameters were first established, and a large number of stochastic samples were generated using Latin hypercube sampling (LHS). Each random sea state sample was used to drive the coupled model, yielding the dynamic responses of three key riser parameters—the effective tension, bending moment, and von Mises stress. Based on predefined failure criteria, the occurrence probability of failure events was statistically estimated to quantify risk. To further identify the relative contributions of environmental factors to riser response risk, a global sensitivity analysis was conducted. Finally, the quantitative results were used to provide practical guidance for structural design optimization, operational strategies, and emergency planning.

3.1. Hydrodynamic Modeling of the Deep-Sea Mining Vessel

Based on an existing multi-purpose vessel (MPV) hull form, a finite element model of the mining vessel was established in ANSYS. Subsequently, a frequency-domain hydrodynamic analysis was conducted using AQWA to obtain the vessel's RAOs under regular wave excitation. The computed RAOs were then imported into OrcaFlex as motion inputs for the vessel, thereby enabling a fully coupled dynamic response analysis with the connected riser system.

In the AQWA simulations, the vessel was modeled as a rigid body, with specified mass properties, a center of gravity location, and hydrostatic parameters. The vessel's moments of inertia were also defined. For regular-shaped ships, the radii of gyration often depend on empirical formulas and can be approximated as follows [50]:

$$\begin{cases} k_{xx} = 0.34 \times B \\ k_{yy} = 0.25 \times L \\ k_{zz} = 0.26 \times L \end{cases} \tag{27}$$

where B is the vessel breadth and L is the vessel length. Based on the radius of gyration, the moment of inertia can be calculated using the following relation:

$$I = mk^2 \tag{28}$$

where I is the moment of inertia, m is the vessel mass, and k is the radius of gyration.

The specific parameters of the mining vessel adopted in this study are summarized in Table 2.

Table 2. The specific parameters of the mining vessel.

Parameter	Value
Length overall (m)	227
Breadth (m)	40
Depth (m)	18.2
Design draft (m)	13.2
Design displacement (t)	68,000

To ensure the accuracy of the hydrodynamic calculations, mesh refinement was applied near the waterline, and uniform meshing was adopted for the submerged hull surfaces. The mesh size for the vessel model was set to 0.8 m. The simulated deep-sea domain was configured as a rectangular basin with a depth of 5000 m and horizontal dimensions of 1000 m $\times$ 1000 m.

In the hydrodynamic simulation of the mining vessel, the wave frequency range was set from 0.04 to 0.5 Hz (equivalent to wave periods of 2 to 25 s), covering the majority of ocean wave frequencies. The wave direction was varied from 0° to 180° in increments of 30°, resulting in seven incident directions.

3.2. Simulation Modeling and Validation of Vessel–Riser Coupling

3.2.1. Vessel–Riser Coupled Simulation Modeling

After obtaining the six-degree-of-freedom RAO values of the mining vessel under wave excitation, these RAOs were used as boundary conditions in the OrcaFlex simulation model of the deep-sea mining system. The environmental parameters used in the simulation are summarized in Table 3.

Table 3. The environmental parameters used in the simulation.

Environmental Parameter	Value
Depth (m)	5000
Sea temperature (°C)	10
Sea density (t/m^3)	1.03
Kinematic viscosity (m^2/s)	1.35×10^{-6}
Seabed stiffness (kN/m/m^2)	100
Air density (kg/m^3)	1.28
Wave type	JONSWAP

The vertical riser and flexible hose models were constructed based on actual geometric dimensions and material properties. The detailed parameters of the rigid riser are provided in Table 4. Since the sizes of the intermediate buffer and lifting pump are both less than 1% of the riser length, they were simplified in the model as pipe elements with equivalent mechanical properties. The mining vessel and seafloor mining vehicle were modeled using the Vessel module in OrcaFlex, while the riser and transport hose system were modeled using the Line module. For the flexible transport hose, a suspended arch-shaped config-

uration was achieved through the implementation of Clump modules, which represent distributed buoyancy modules.

Table 4. The detailed parameters of the rigid riser.

Parameter	Value
Inner diameter (mm)	204
Outer diameter (mm)	244
Length (m)	5000
Weight in water (kg/m)	112.5
Yield strength (Mpa)	758 (σ_{bmin}), 965 (σ_{bmax})
Elastic modulus (kPa)	2.12×10^8
Material density (kg/m^3)	7850

3.2.2. Convergence and Discretization Analysis

To evaluate the stability and reliability of the proposed deep-sea mining system simulation model, a convergence analysis was performed. Specifically, the time step size of the riser model was systematically varied while keeping the environmental conditions constant. The simulations were conducted for a duration of 50 s with time steps of 0.01 s, 0.05 s, 0.1 s, 0.5 s, and 1.0 s. The convergence was assessed by examining the variations in the maximum values of three key dynamic response parameters of the riser upon completion of the dynamic calculations.

The maximum values of the effective tension, bending moment, and von Mises stress of the riser under different time step sizes are summarized in the Table 5, with the smallest time step (0.01 s) taken as the reference solution. When the time step was set to 1.0 s, the bending moment exhibited the largest relative error of 4.2463%, while the relative errors for all other time steps remained below 1%. With the reduction in the time step, the relative errors of the three dynamic response parameters consistently decreased and converged toward stable values. These results indicate good convergence and demonstrate the numerical stability of the proposed simulation model. To ensure a balance between computational efficiency and accuracy, a time step of 0.1 s was selected for subsequent analyses.

Table 5. Variation of riser dynamic response parameters under different time steps.

Time Step (s)		Value	Relative Error (%)
0.01	Effective tension (kN)	5723.8628	/
	Bend moment (kN·m)	3.0709	/
	Von Mises stress (kPa)	406,688.1726	/
0.05	Effective tension (kN)	5723.9961	0.0023
	Bend moment (kN·m)	3.0652	0.1856
	Von Mises stress (kPa)	406,697.6438	0.0023
0.1	Effective tension (kN)	5722.7754	0.0190
	Bend moment (kN·m)	3.0773	0.2084
	Von Mises stress (kPa)	406,610.9111	0.0190
0.5	Effective tension (kN)	5699.645	0.4231
	Bend moment (kN·m)	3.0385	1.0550
	Von Mises stress (kPa)	404,967.4705	0.4231
1	Effective tension (kN)	5671.2593	0.9190
	Bend moment (kN·m)	2.9405	4.2463
	Von Mises stress (kPa)	402,950.626	0.9190

In OrcaFlex, line-type objects such as risers are discretized by specifying the segment length. To assess the numerical accuracy of the riser model under spatial discretization,

a convergence study was further performed with segment lengths of 12.5 m, 10 m, 7.5 m, 5 m, 2.5 m, and 1.25 m. The key structural response parameters examined included the effective tension, bending moment, and Von Mises stress. The results obtained with the finest discretization (1.25 m) were treated as the reference solution, against which the relative errors of other segment lengths were evaluated.

The maximum values of the effective tension, bending moment, and von Mises stress of the riser under different segment lengths are summarized in Table 6. It can be observed that the relative errors in effective tension and von Mises stress are extremely small (<0.001%), indicating that these responses are largely insensitive to riser segmentation. In contrast, the bending moment gradually converges to a stable value as the segment length decreases, confirming the numerical consistency of the model under spatial discretization. The relative error at a segment length of 12.5 m reaches 27.0344%, whereas it decreases to 1.6715% at 2.5 m, which lies within an acceptable engineering range. This observation indicates that the bending moment, as a local response parameter, is more sensitive to segment length and requires sufficiently fine discretization to obtain reliable results. Considering both simulation efficiency and discretization accuracy, a segment length of 2.5 m was adopted for the riser model in this study.

Table 6. Variation of riser dynamic response parameters under different segment length.

Segment Length (m)		Value	Relative Error (%)
1.25	Effective tension (kN)	5722.7827	/
	Bend moment (kN·m)	3.9844	/
	Von Mises stress (kPa)	406,611.4309	/
2.5	Effective tension (kN)	5722.7822	<0.001%
	Bend moment (kN·m)	3.9178	1.6715
	Von Mises stress (kPa)	406,611.3963	<0.001%
5	Effective tension (kN)	5722.7808	<0.001%
	Bend moment (kN·m)	3.5643	10.5436
	Von Mises stress (kPa)	406,611.2923	<0.001%
7.5	Effective tension (kN)	5722.7788	<0.001%
	Bend moment (kN·m)	3.2899	17.4305
	Von Mises stress (kPa)	406,611.1537	<0.001%
10	Effective tension (kN)	5722.7754	<0.001%
	Bend moment (kN·m)	3.0773	22.8491
	Von Mises stress (kPa)	406,610.9111	<0.001%
12.5	Effective tension (kN)	5722.7715	<0.001%
	Bend moment (kN·m)	2.9072	27.0344
	Von Mises stress (kPa)	406,610.6340	<0.001%

The convergence analyses with respect to both the time step size and spatial discretization demonstrate that the proposed deep-sea mining system simulation model is numerically stable and reliable. The key dynamic and structural responses of the riser, including the effective tension, bending moment, and Von Mises stress, converge consistently toward stable values as the time step decreases and the segment length is refined. While the effective tension and Von Mises stress are largely insensitive to discretization, the bending moment, as a more localized response, shows higher sensitivity and requires sufficiently fine temporal and spatial resolutions. Based on these results, a time step of 0.1 s and a segment length of 2.5 m were selected, providing a good balance between computational efficiency and accuracy. Overall, these findings validate the numerical correctness of the simulation model and support its use for subsequent analyses.

3.3. Uncertainty Modeling and Sample Generation

To estimate the structural failure probability and reliability indices—and to further quantify the sensitivity of system responses to various uncertain ocean environmental parameters—it is essential to establish probabilistic distribution models for these uncertainties and generate large-scale samples before the Monte Carlo simulation.

In constructing the Monte Carlo simulation framework, uncertainty modeling of ocean environmental parameters is based on engineering experience and statistical data, with appropriate probability distributions selected accordingly. The wave height, being non-negative and exhibiting long-tail characteristics—with a non-negligible probability of extreme values—is modeled using the Weibull distribution. The wave direction is assumed to follow a uniform distribution, reflecting the equal likelihood of wave incidence from all directions. For simplification, both current and wind directions are assumed to be aligned with the wave direction, which is consistent with the directional correlation often observed in wind–wave–current conditions in offshore environments. The current speed is modeled using a triangular distribution, which effectively captures the bounded nature of current speeds and their central tendency, aligning with measured current statistics in deep-sea regions. The wind speed is modeled by a log-normal distribution to reflect its right-skewed and heavy-tailed nature, in agreement with empirical wind data from marine observations.

Empirical studies and engineering experience suggest that the wave height and wave period are statistically correlated in deep-sea mining zones; in general, higher waves are associated with longer periods. This correlation originates from wave energy propagation mechanics and generation processes. To ensure that sampled scenarios remain physically realistic, this statistical dependency must be preserved in the sampling process. While a deterministic or linear relationship can be assumed in some cases, such strong coupling may obscure the results of the sensitivity analysis. Therefore, in this study, a nonlinear conditional mean function is employed to determine the wave period corresponding to each sampled wave height. A power-law function is selected to represent the nonlinear trend between the wave height and period, with small random perturbations introduced to account for variability. The detailed parameters for each probability distribution are listed in Table 7, while the extreme sea states referenced in this study are based on wave and current statistics from the South China Sea, as provided by the Offshore Oil Research Center (Table 8).

Table 7. The detailed parameters for each probability distribution model.

Uncertain Environmental Parameter	Probability Distribution Model
Wave heigh t(m)	$H_s \sim Weibull(\lambda = 3.5, k = 2), H_s \in [0.5, 15]$
Wave period (s)	$T_p = 1.1 \times H_s + \varepsilon, \varepsilon \sim N(0,1), T_p \in [4, 18]$
Wave direction (°)	$\theta \in [0, 360]$, uniform
Current speed (m/s)	$V_c \sim Triangular, V_c \in [0.1, 2]$
Wind speed (m/s)	$V_w \sim Lognormal(mean = 15, \sigma = 0.5), V_w \in [4, 50]$

Table 8. Wave and current parameters of the South China Sea under extreme sea conditions.

Sea State Parameters	Sea State 1 (Once in 100 Years)	Sea State 2 (Once in 200 Years)	Sea State 3 (Once in 500 Years)
Wave Height (m)	13.3	13.7	14.2
Wave Period (s)	15.5	16	16.6
Current Speed (m/s)	1.97	2.05	2.13

Latin hypercube sampling (LHS), a widely used stratified sampling technique in Monte Carlo-based uncertainty quantification and reliability analyses [51], is employed to generate 10,000 samples encompassing the wave height, wave period, wave direction,

current speed, and wind speed. The marginal distributions of the sampled parameters are shown in Figure 3a–e, with the nonlinear relationship between the wave height and wave period illustrated in Figure 3f.

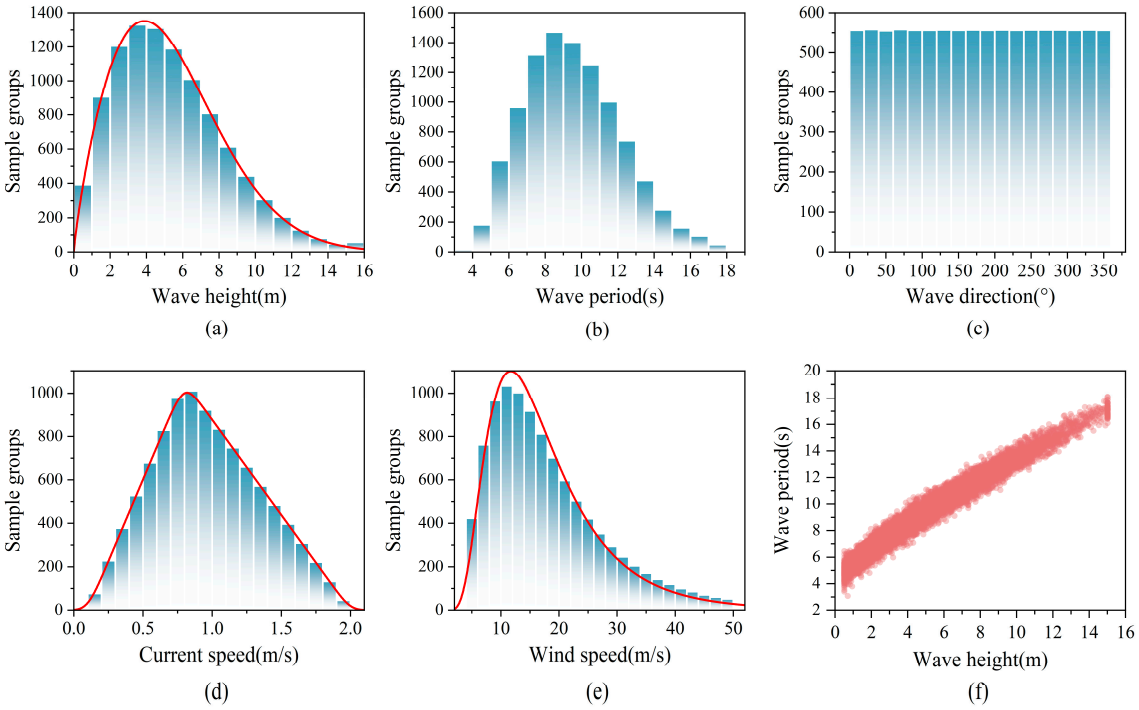


Figure 3. Sample distributions of the ocean parameters: (**a**) distribution of wave height samples; (**b**) distribution of wave period samples; (**c**) distribution of wave direction samples; (**d**) distribution of current speed samples; (**e**) distribution of wind speed samples; (**f**) nonlinear relationship between the wave height and wave period.

3.4. Failure Criteria Definition

The calculation of response limit values is performed following the API RP 2RD standard [52], which adopts a two-thirds yield strength criterion in combination with a design condition factor C_f. This regulatory framework is particularly suitable for evaluating the safety of deep-sea risers subjected to tension-bending coupled loading, which governs their structural performance.

The allowable von Mises stress is defined by:

$$\sigma_{allow} = C_f \cdot \frac{2}{3} \cdot \sigma_y \tag{29}$$

In this study, the riser is constructed using P110-grade steel, with material yield strength σ_y values ranging from 758 MPa to 965 MPa. According to API RP 2RD, the design factor C_f is set to 1.0 under normal operational conditions.

The maximum allowable effective tension of the riser is determined based on the von Mises yield criterion and calculated as:

$$T_{lim} = A \cdot \sigma_{allow} = A \cdot \left(C_f \cdot \frac{2}{3} \cdot \sigma_y \right) \tag{30}$$

where A is the effective cross-sectional area of the riser, defined for an annular section as:

$$A = \frac{\pi}{4} \left(D^2 - d^2 \right) \tag{31}$$

The maximum allowable bending moment is evaluated based on the yield strength and the section modulus Z of the riser, as follows:

$$M_{lim} = Z \cdot \sigma_{allow} = Z \cdot \left(C_f \cdot \frac{2}{3} \cdot \sigma_y \right) \tag{32}$$

For a circular cross-section, the section modulus is given by:

$$Z = \frac{\pi}{32} \cdot \frac{D^2 - d^2}{D} \tag{33}$$

The computed maximum allowable values for effective tension, bending moment, and von Mises stress are summarized in Table 9.

Table 9. The computed maximum allowable values for dynamic response of deep-sea mining risers.

Parameter	Failure Criteria Value
Maximum allowable effective tension (kN)	7112
Maximum bending moment (kN·m)	368
Maximum allowable von Mises stress (kPa)	505,000

3.5. Sensitivity Analysis

To identify the dominant environmental factors influencing the riser response, this study employs the Spearman rank correlation coefficient as a surrogate for the first-order Sobol sensitivity index. This approach captures the nonlinear monotonic relationship between each uncertain sea state parameter and the riser's structural response, while computing the corresponding p-values to assess the statistical significance of the correlations. In addition, a second-order response surface regression model is constructed to establish a multi-input–single-output sensitivity analysis framework.

Generally, if $p < 0.05$, the correlation is considered statistically significant; if $p < 0.001$, the correlation is regarded as highly significant and statistically robust. Conversely, when $p \geq 0.05$, it indicates that the sample data do not provide sufficient evidence to confirm a statistically meaningful relationship between the input variable and structural response, suggesting the observed correlation may result from random variability.

Additionally, special consideration is given to the wave direction, which is a cyclical variable ranging from 0° to 360°. Directly using its numeric values in Sobol-type sensitivity analyses would lead to inaccurate results, as angles such as 0° and 360°, or 90° and 270°, are physically equivalent in terms of directional excitation on the riser but numerically distant. To address this, the wave direction is vectorized using a trigonometric transformation, where it is represented by two continuous variables:

$$\begin{cases} X_{cos} = cos(\theta \times \pi/180) \\ X_{sin} = sin(\theta \times \pi/180) \end{cases} \tag{34}$$

The variables X_{cos} and X_{sin} represent the horizontal and vertical projections of the wave direction on the unit circle, respectively, with value ranges normalized to $[-1, 1]$. This transformation effectively eliminates the periodic discontinuity of directional angles, allowing the sensitivity analysis to more accurately quantify the influence of the wave direction on the structural responses of the riser system.

4. Results and Discussion

4.1. Results

4.1.1. Hydrodynamic Analysis of the Deep-Sea Mining Vessel

After completing the simulation setup and execution, Figure 4 presents the vessel motion response spectra based on RAOs for each degree of freedom. The RAO curves exhibit clear directional sensitivity, particularly in the roll and heave responses. Under combined wave action, the RAO values for the vessel's six degrees of freedom generally decrease with increasing wave frequency. When the frequency exceeds 0.2 Hz, the RAO values for heave, pitch, roll, and surge gradually approach zero, indicating that high-frequency disturbances are dominated by system inertia. Peak RAO values for heave, pitch, roll, and yaw occur around 0.1 Hz, demonstrating distinct resonance behavior and high sensitivity to wave incident angles. The motion responses in heave, roll, and sway are significantly amplified under 90° wave directions, indicating that transverse wave excitation is strongest under beam seas. For the surge, prominent motion responses are observed near 0.05–0.08 Hz at 180°, consistent with the characteristics of wave drift forces and low-frequency excitation under head seas. The responses of pitch and yaw are significantly amplified when waves approach from 120°, reflecting directional dependence in the vessel's rotational behavior.

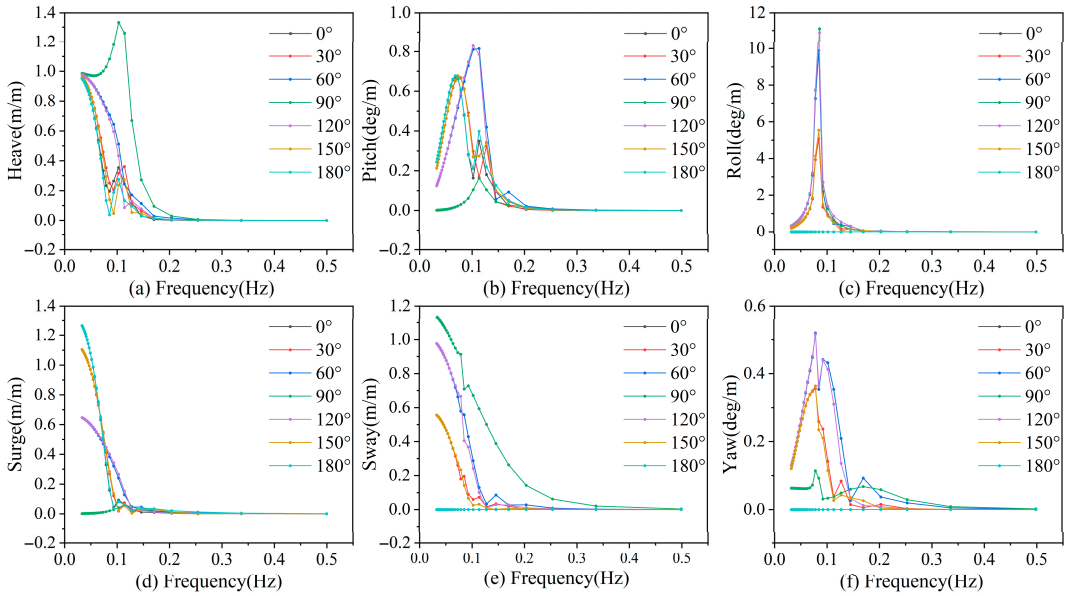


Figure 4. The motion RAOs of the mining vessel in surge, sway, heave, roll, pitch, and yaw: (**a**) RAOs of heave motion under different wave directions; (**b**) RAOs of pitch motion under different wave directions; (**c**) RAOs of roll motion under different wave directions; (**d**) RAOs of surge motion under different wave directions; (**e**) RAOs of sway motion under different wave directions; (**f**) RAOs of yaw motion under different wave directions.

4.1.2. Analysis of Influencing Factors on Dynamic Behavior

To investigate effects of multiple ocean environmental factors on the dynamic response of the deep-sea mining riser under vessel–riser coupling conditions, this study examines the variations in effective tension, bending moment, and von Mises stress in the riser under different wave heights, wave periods, wave directions, current velocities, and wind speeds. In practice, deep-sea mining systems typically operate under normal sea conditions; therefore, all environmental parameters selected for simulation fall within ranges commonly observed in real-world marine operations.

The effective tension, bending moment, and von Mises stress of the riser were obtained through OrcaFlex simulations. These three parameters were selected as key indicators because they represent the primary failure mechanisms of the riser system, namely the axial stiffness (effective tension), bending deformation (bending moment), and multiaxial stress coupling (von Mises stress). Their magnitudes directly determine the occurrence of tensile failure, buckling, excessive bending, or fatigue.

For a wave period of 10 s, wave direction of 0°, current speed of 1 m/s, and wind speed of 25 m/s, the wave heights varied between 5 and 8 m. The corresponding results are shown in Figure 5. The results show that the effective tension, bending moment, and von Mises stress increase with the wave height. All three response metrics follow consistent trends across different wave heights. At wave heights of 8 m and 5 m, the maximum effective tensions are 5775.5 kN and 5694.2 kN, differing by 1.42%; the maximum bending moments are 3.1842 kN·m and 3.0805 kN·m, differing by 3.36%; and the maximum von Mises stresses are 410,360.2 kPa and 404,581.3 kPa, a difference of 1.43%.

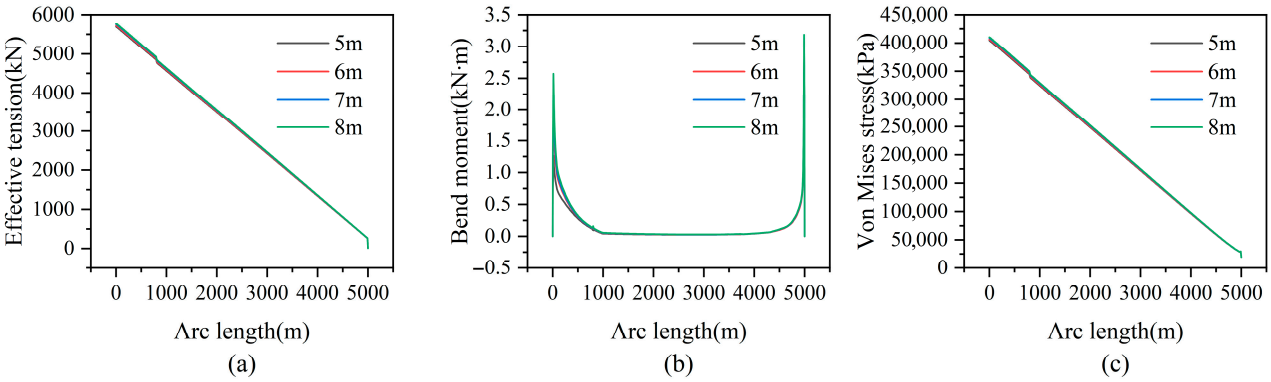


Figure 5. Impact of wave height variation on the riser dynamic response: (**a**) distribution of effective stress values along the riser under different wave heights; (**b**) distribution of bending moments along the riser under different wave heights; (**c**) distribution of von Mises stress values along the riser under different wave heights.

With the wave height set to 6 m, wave direction to 0°, current speed to 1 m/s, and wind speed to 25 m/s, different wave periods were investigated to evaluate their influence on the riser's responses. As shown in Figure 6, the influence of the wave period on the effective tension, bending moment, and von Mises stress remains significant. When the wave periods are 12 s and 9 s, the maximum effective tensions are 5824.3 kN and 5763.3 kN, differing by 1.06%; the corresponding maximum bending moments are 3.3331 kN·m and 3.1521 kN·m, differing by 5.74%; and the maximum von Mises stresses are 413,828.7 kPa and 409,491.9 kPa, a difference of 1.06%.

Next, the wave direction was varied from 0° to 90° in 30° increments, while the wave height was maintained at 6 m and the wave period at 10 s. Other environmental parameters remained unchanged. The resulting changes in effective tension, bending moment, and von Mises stress are shown in Figure 7. All three responses vary significantly with the wave direction. At a wave direction of 90°, the values of the effective tension, bending moment, and von Mises stress attain their maximum values. This indicates that when waves strike the vessel laterally (beam-on orientation), the vessel undergoes the largest rolling motion, causing the top of the riser to sway laterally, which in turn leads to intensified bending and increased effective tension. Specifically, the maximum effective tensions at 90° and 0° are 6253.1 kN and 5722.8 kN, a difference of 9.27%; the maximum bending moments are 3.8949 kN·m and 3.0773 kN·m, differing by 26.57%; and the maximum von Mises stresses are 444,288.5 kPa and 406,610.9 kPa, with a 9.27% difference.

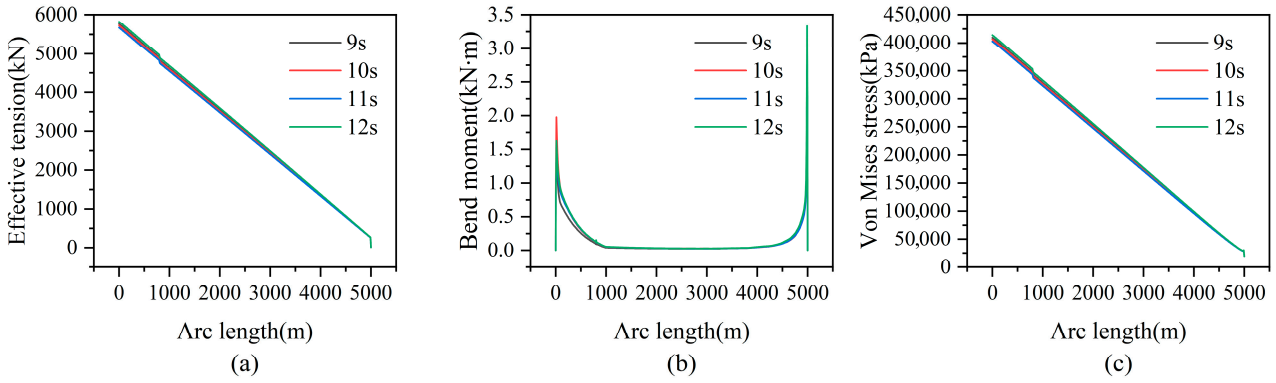


Figure 6. Impact of wave period variation on the riser dynamic response: (**a**) distribution of effective stress values along the riser under different wave periods; (**b**) distribution of bending moments along the riser under different wave periods; (**c**) distribution of von Mises stress values along the riser under different wave periods.

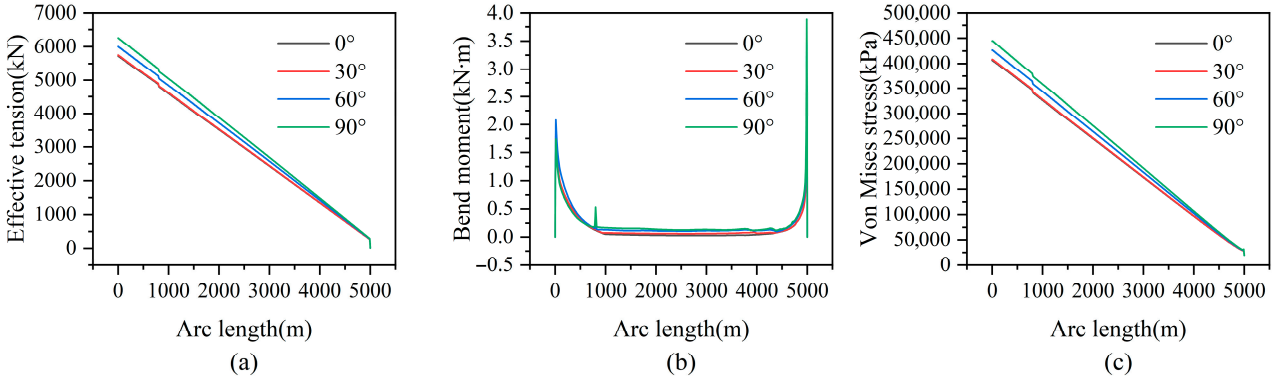


Figure 7. Impact of wave direction variation on the riser dynamic response: (**a**) distribution of effective tension values along the riser under different wave directions; (**b**) distribution of bending moment values along the riser under different wave directions; (**c**) distribution of von Mises stress values along the riser under different wave directions.

Finally, keeping the wave height fixed at 6 m, wave period at 10 s, wave direction at 0°, and wind speed at 25 m/s, the surface current speed was varied. The resulting riser responses are presented in Figure 8. It can be observed that current speed has a significant influence on the bending moment but a relatively minor effect on the effective tension and von Mises stress. This can be attributed to the long length of the riser, which amplifies small lateral disturbances, resulting in a pronounced transverse curvature and lateral displacement in the midsection of the riser. In contrast, axial tension generally dominates the effective tension in deep-sea mining risers, and lateral currents do not directly induce axial forces or cause large vessel displacements that would alter the effective tension. Since the von Mises stress is also primarily governed by axial tension, its variation remains limited. For instance, at current speeds of 2 m/s and 0.5 m/s, the maximum effective tensions are 5724.7 kN and 5711.6 kN, differing by only 0.23%. However, the maximum bending moments increase significantly with the current speed, reaching 4.3046 kN·m and 2.9296 kN·m, respectively—a difference of 46.93%. The corresponding maximum von Mises stresses are 406,747.5 kPa and 405,810.4 kPa, differing by 0.23%.

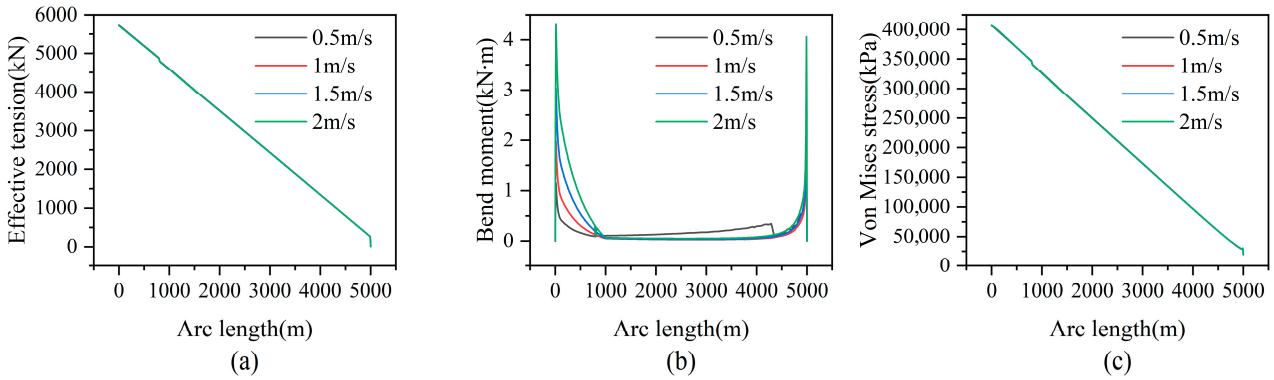


Figure 8. Impact of current speed variation on the dynamic riser response: (**a**) distribution of effective tension values along the riser under different current speeds; (**b**) distribution of bend moment values along the riser under different current speeds; (**c**) distribution of von Mises stress values along the riser under different current speeds.

In addition, extensive simulation results demonstrate that variations in wind speed have a minimal impact on the dynamic behavior of the deep-sea mining riser under vessel–riser coupled conditions. This phenomenon can be primarily attributed to the wave modeling methodology adopted in OrcaFlex, which is based on the JONSWAP wave spectrum. Within this framework, wind is treated as the primary energy source for wave generation and spectral evolution, rather than as a direct mechanical load acting on the vessel or riser structure. As a parametric model, the JONSWAP spectrum describes the energy distribution of ocean waves under finite wind fetch conditions, and the effects of wind are indirectly incorporated through parameters such as the spectral shape and peak enhancement factor. Therefore, unless the aerodynamic forces or wind-induced surface currents are explicitly coupled in the simulation model, the direct mechanical influence of wind on the riser remains extremely limited. Furthermore, due to the nearly vertical configuration of the riser and its minimal projected area above the water surface, the wind-induced aerodynamic forces are considerably smaller than the hydrodynamic loads induced by waves and currents. This explains why changes in wind speed exert negligible influence on the riser's effective tension, bending moment, and stress distribution.

From the analysis of Figures 4–7, it can be observed that the effective tension in the riser gradually decreases from the top to the bottom, with the maximum value located at the top end connected to the mining vessel. This is primarily due to the accumulation of self-weight and internal fluid loads in the upper section, compounded by the multi-degree-of-freedom motion of the vessel under wave action, which transmits dynamic tension directly to the riser's top segment.

The bending moment exhibits prominent peaks near the top and bottom of the riser. In contrast, the midsection experiences significantly lower bending moments. This spatial distribution indicates that the lateral displacement of the riser is more pronounced at the top and bottom, where boundary interactions are strongest. At the top, the riser is subjected to the vessel's complex motion with low resistance, resulting in concentrated inertial forces and bending moment peaks. At the bottom, the mass of the intermediate buffer exerts an inertial reaction, contributing to localized bending moment amplification.

The von Mises stress shows a distribution pattern consistent with that of effective tension, indicating that axial stress induced by tension is the dominant contributor. The contribution of bending and shear stresses is relatively small, given the high slenderness ratio and tension-dominated state of the riser. This behavior highlights that the top region of the riser is a potentially critical area for structural failure and should be the focus of structural design and reliability assessment to ensure adequate safety margins.

4.1.3. Riser Response Analysis Based on Monte Carlo Simulation

Although Section 4.1.2 systematically analyzed the dynamic response characteristics of the riser under various typical sea states through a controlled variable approach, such deterministic simulations represent only discrete and limited operating conditions. As such, they are insufficient to fully capture the inherent uncertainty of the ocean environment or its cumulative effect on system safety. While it is evident that various environmental loads exert significantly different impacts on the dynamic response of the riser under vessel–pipe coupling, the degree to which these uncertain factors contribute to structural risk cannot be directly inferred. To quantitatively assess the dynamic behavior risks of the riser across uncertain sea state parameters, and to distinguish the relative influence of each factor, a Monte Carlo simulation method grounded in probabilistic statistical theory is introduced. This enables a transition from a deterministic response analysis to probabilistic risk evaluation.

An integrated simulation platform was developed by coupling OrcaFlex with MATLAB R2024b using the OrcFxAPI module, allowing automated setup and batch execution of simulation cases directly from MATLAB. Within this platform, MATLAB manages the input parameter generation and execution control, while OrcaFlex performs the dynamic response analysis of the deep-sea mining vessel–riser coupled system. After completing the co-simulation, the maximum values of the effective tension, bending moment, and von Mises stress are extracted from each case for a further statistical analysis.

The scatter plots of dynamic extreme responses against ocean parameters—namely the wave height, wave period, wave direction, current speed, and wind speed—are shown in Figure 9. These plots demonstrate how the maximum effective tension, bending moment, and von Mises stress vary in response to changes in environmental conditions across a large number of samples. Overall, the responses tend to increase with the rising wave height and wave period, indicating a strong positive correlation. Additionally, all three responses exhibit noticeable peaks when the wave direction approaches 90° and 270°, especially evident in the effective tension (Figure 9a) and von Mises stress (Figure 9c). This highlights that lateral wave loading, especially from beam seas, significantly amplifies vessel motions, which in turn strongly affect the riser tension and stress response. These trends are consistent with the deterministic results presented in Section 3.2.2.

Moreover, Figure 9b shows a clear upward trend in the bending moment with increasing current speeds. This behavior is attributed to the long and slender geometry of the riser deployed at depths of several kilometers, making it highly sensitive to lateral currents. In contrast, the effective tension and von Mises stress do not exhibit a similarly consistent pattern with the current speed, as their magnitudes are primarily governed by axial loading and vessel-induced dynamics rather than horizontal hydrodynamic drag.

With respect to wind speed, its influence on both the riser bending moment and von Mises stress is significantly less pronounced than that of wave-related parameters, displaying an almost random scatter. This suggests that under the current modeling assumptions, wind effects are primarily embedded in the wave generation process via the JONSWAP spectrum and do not directly impose dynamic forces on the riser. Consequently, the riser's axial and bending responses remain insensitive to variations in wind speed. While more complex nonlinear or time-lagged coupling mechanisms may exist between the wind and riser response, such effects are not captured in the present study, which assumes static and decoupled wind input conditions.

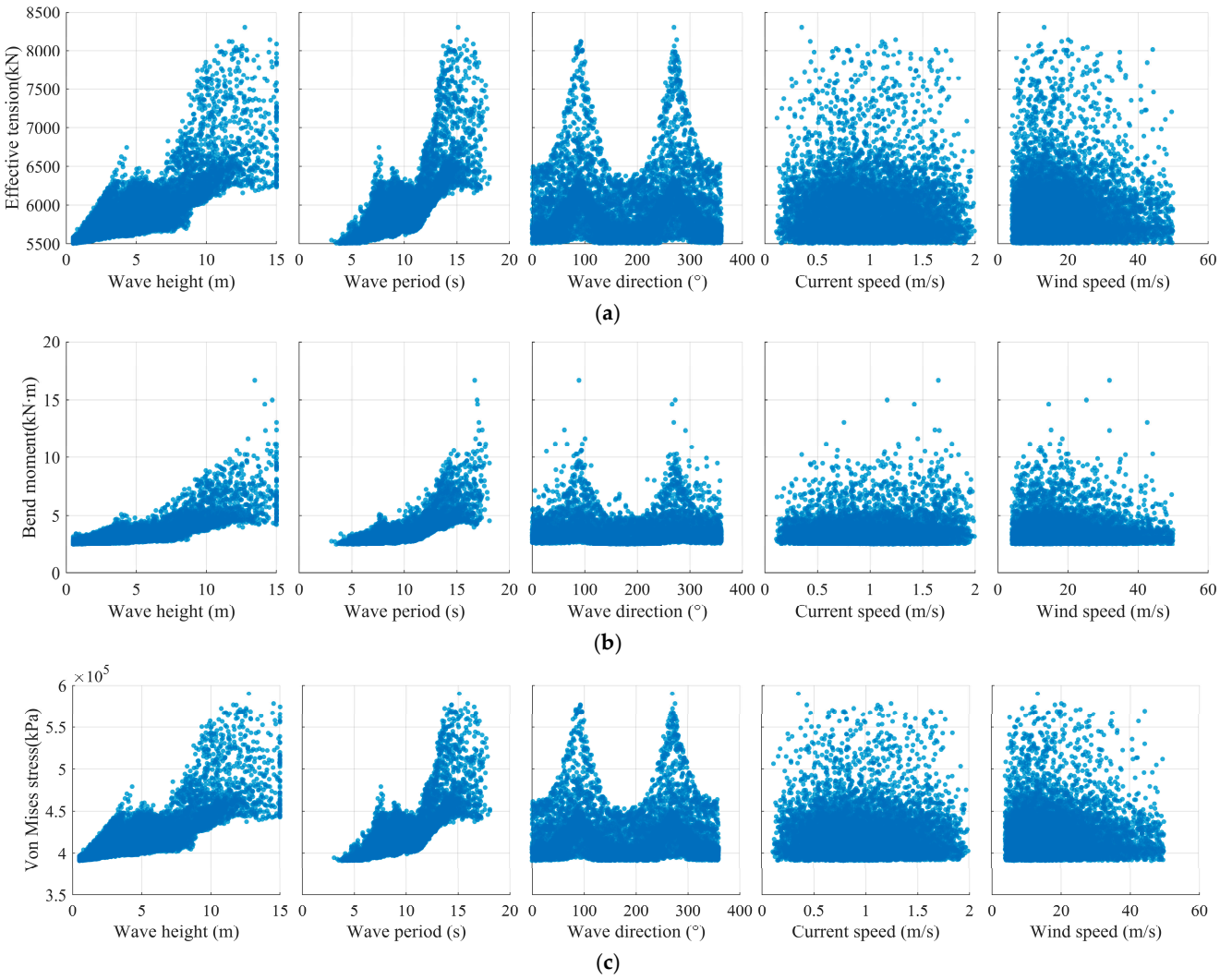


Figure 9. Scatter plots of dynamic extreme responses versus ocean parameters: (**a**) sample distribution of the maximum effective stress with the wave height, wave period, wave direction, current speed, and wind speed; (**b**) sample distribution of the maximum bending moment with the wave height, wave period, wave direction, current speed, and wind speed; (**c**) sample distribution of the maximum von Mises stress with the wave height, wave period, wave direction, current speed, and wind speed.

4.1.4. Reliability Analysis

By constructing the probability density functions (PDFs) of riser response variables, the central tendency, dispersion, and skewness of structural responses can be characterized. Comparing these PDFs with corresponding failure thresholds enables estimations of the proportion of samples falling within the failure domain.

Figure 10 presents the PDFs of the maximum effective tension, bending moment, and von Mises stress of the mining riser obtained through Monte Carlo simulations. The results are fitted using log-normal distributions. The response distributions exhibit significant positive skewness, with probabilities decreasing rapidly as the response values increase, emphasizing the dominant role of rare extreme events in the dynamic behavior of deep-sea mining risers under stochastic marine loads. The log-normal distribution fits well with the simulation data in all three cases, indicating its suitability for capturing the probabilistic characteristics of the structural responses.

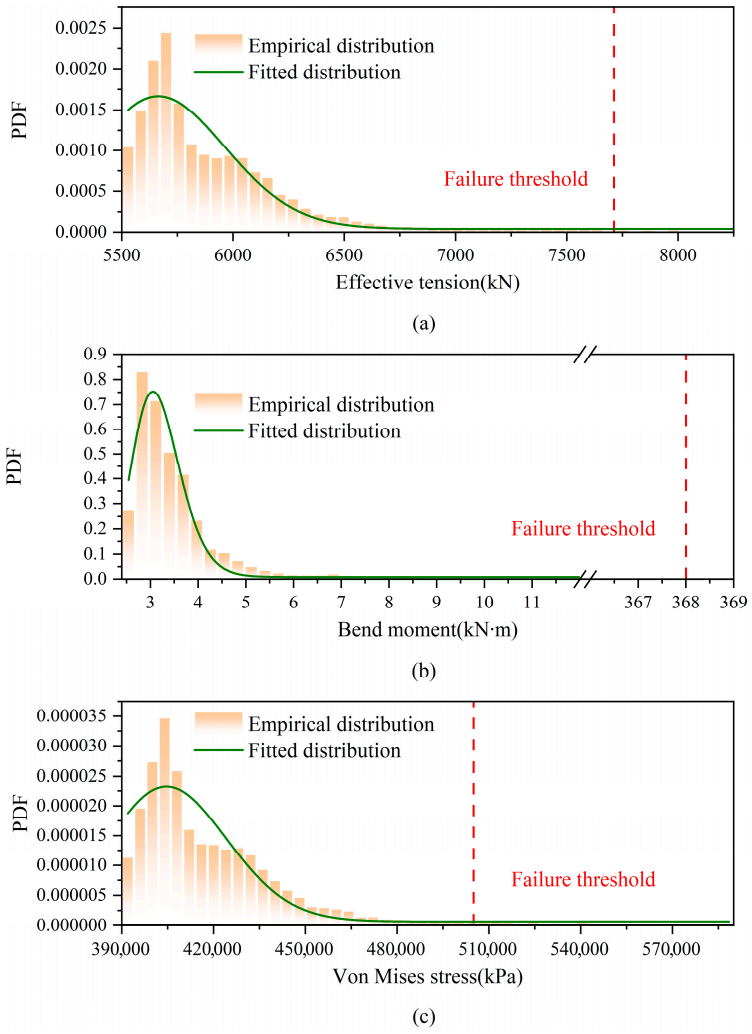


Figure 10. PDFs of the riser dynamic response with fitted distribution: (**a**) PDF and fitting of maximum effective stress values with the failure threshold; (**b**) PDF and fitting of maximum bend moment values with the failure threshold; (**c**) PDF and fitting of maximum von Mises stress values with the failure threshold.

In Figure 10a, the distribution of effective tension shows a typical right-skewed shape. Most samples are concentrated in the range of 5600–6400 kN, and the majority remain within the allowable tension limit. However, a few rare samples approach or exceed the threshold under extreme sea states, indicating a non-negligible tension-induced failure probability.

In Figure 10b, the distribution of maximum bending moments shows that most values lie between 3 and 6 kN·m. The tail is long but sparse, and the failure threshold is set at 358 kN·m, which is significantly higher than the observed values. This implies that the probability of bending-induced failure is extremely low, and the system is structurally safe in terms of bending performance.

Figure 10c illustrates the PDF of von Mises stress values, which shows a distribution pattern similar to that of effective tension. The peak probability density is located around 400 MPa, and the tail decays rapidly before reaching the failure limit, indicating that the principal stress is dominated by axial loading and that the risk of failure due to von Mises stress remains minimal under most conditions.

Based on the Monte Carlo simulation with 10,000 samples under the vessel–riser coupling effects, the structural failure probabilities and reliability indices of the deep-sea mining riser were evaluated. The results are summarized in Table 10.

Table 10. The structural failure probabilities and reliability indices of the deep-sea mining riser.

Response Parameter	Failure Probability	Reliability Index
Effective tension	2.15%	2.02
Bend moment	0.01%	3.72
Von Mises stress	2.19%	2.02

The analysis indicates that the riser exhibits high structural safety against bending-dominated failure modes, while tension- and stress-dominated failure modes warrant increased attention. The moderate reliability indices observed for effective tension and von Mises stress suggest that although the current design remains within acceptable safety margins, potential risks may arise under extreme environmental conditions or long-term service.

Therefore, it is recommended to enhance the riser stiffness or adopt structural compensation strategies in future design iterations for improved overall system reliability and robustness. Based on the derived probability distribution results, it is also advisable to implement real-time monitoring of effective tension and bending moment values at critical locations of the riser, such as the top connection to the vessel and the bottom connection to the intermediate buffer. Warning thresholds may be set at 80% to 90% of the design limits to trigger riser retrieval or system shutdown procedures, accounting for model uncertainty and rare extreme conditions not fully captured in simulations. Additionally, if the measured effective tension approaches the dynamic amplification regions identified in the time-domain analysis, or if the significant wave height exceeds a pre-defined threshold, such as 12 m, operational restrictions are advised. These engineering strategies aim to ensure riser safety while maintaining operational efficiency and extending the service life, ultimately reducing the risk of structural failure under coupled environmental loading.

4.1.5. Parameter Sensitivity Analysis

In the sensitivity analysis of uncertain ocean parameters, wind speed is excluded. Due to the nature of the wave spectrum, the effect of wind is indirectly embedded in the spectral parameters rather than acting as an explicit mechanical input. Both the modeling assumptions and the results in Section 4.1.2 confirm that wind speed has a negligible influence on the riser's structural behavior. Therefore, its exclusion from further sensitivity evaluations is justified.

As illustrated in Figure 11, the sensitivity indices of each uncertain environmental parameter on the riser's structural responses are shown. The corresponding sensitivity values and statistical p-values are summarized in Table 11. The wave height and wave period exhibit the highest sensitivity across all structural responses, including effective tension, bending moment, and von Mises stress values. This indicates that these two wave parameters play a dominant role in influencing the dynamic behavior of the riser system.

Table 11. Sensitivity indices and p-values of riser responses to ocean parameters.

Response Parameter		H_s	T_p	X_{cos}	X_{sin}	V_c
Effective tension	Sensitivity	0.785	0.770	0.074	0.008	0.013
	p	<0.0001	<0.0001	<0.0001	0.4390	0.2065
Bend moment	Sensitivity	0.772	0.759	0.202	0.005	0.111
	p	<0.0001	<0.0001	<0.0001	0.6310	<0.0001
Von Mises stress	Sensitivity	0.785	0.770	0.073	0.008	0.010
	p	<0.0001	<0.0001	<0.0001	0.4381	0.3073

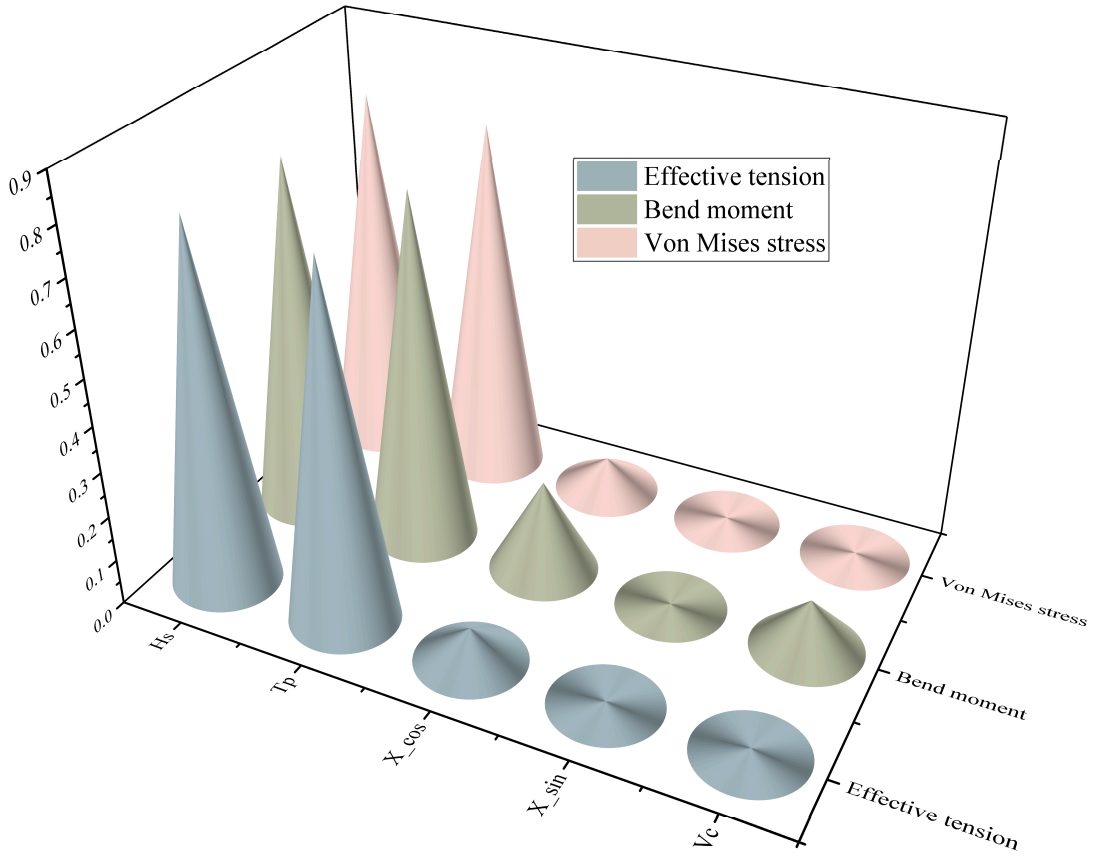


Figure 11. The sensitivity indices of each uncertain environmental parameter on the riser's structural responses.

In addition, the sensitivity index of the X_{cos} component—representing the horizontal projection of the wave direction—is also relatively high. Specifically, when waves propagate from 0° or 180°, corresponding to the longitudinal direction of the structure, $cos(\theta)$ approaches ± 1 and $sin(\theta)$ approaches 0, whereas for 90° or 270°, representing the transverse direction, $cos(\theta)$ approaches 0 and $sin(\theta)$ approaches ± 1. The high sensitivity of X_{cos}, thus, suggests that the riser exhibits stronger structural responses under transverse wave incidence, which typically induces stronger lateral motions and dynamic amplification.

Overall, this analysis confirms that the wave action—rather than ocean currents—is the primary driver of dynamic loading on the deep-sea mining riser. Nevertheless, it is worth noting that current speed also shows a moderately high sensitivity index concerning the bending moment, highlighting its influence on lateral deflection in long, slender riser systems. These findings align with the trends observed in the full-sample distributions discussed in Section 4.1.3, further validating the robustness and reliability of the sensitivity analysis results.

Based on the sensitivity analysis results, optimization efforts should focus on those environmental parameters that exhibit high structural response sensitivity. The wave height and wave period are identified as the most influential environmental factors affecting the effective tension, bending moment, and von Mises stress in the deep-sea mining riser. This highlights the critical role of wave characteristics in governing the dynamic response and structural safety of the riser system. In practical engineering applications, it is recommended to prioritize accurate predictions and statistical modeling of wave conditions in the deployment region. During riser design optimization, particularly for critical locations prone to response amplification (riser top connection), sufficient safety margins should be reserved to account for extreme wave conditions.

In addition, the cosine component of the wave direction (X_{cos}) exhibits high sensitivity, indicating that transverse waves (90° or 270°) induce significantly stronger structural responses compared to longitudinal waves (0° or 180°). This suggests that during operational deployment, the orientation of the riser and mining vessel relative to prevailing wave directions should be carefully considered. The vessel's dynamic positioning system should be used to maintain the bow wave angle within 30°, minimizing exposure to beam sea conditions during mining operations.

Although the current speed shows relatively low overall influence, its notable sensitivity to the bending moment cannot be overlooked, especially in long-duration operations or regions with significant tidal variation. Therefore, real-time monitoring of the current speed is recommended as part of the environmental observation and risk control strategy.

In summary, wave-induced loads are the primary drivers of riser dynamic behavior. Design and control strategies for deep-sea mining systems should focus on mitigating wave effects, such as through the integration of structural dampers, flexible joints, or active positioning systems, to enhance the system's resilience against environmental disturbances.

4.2. Discussion

4.2.1. Comparative Analysis and Advantages

To highlight the advantages of applying Monte Carlo simulations in the risk analyses of deep-sea mining risers, this study compares five representative studies that investigated the dynamic responses of coupled vessel–riser systems under combined ocean environmental loads. Table 12 provides a summary of the comparative analysis between the present study and these representative studies.

Some results of this study indicate that the wave height, wave frequency, and wave direction are the dominant factors influencing riser responses, which is consistent with findings from several representative studies. However, compared with existing work, this study incorporates a more comprehensive set of ocean environmental uncertainties, including the wave height, wave frequency, wave direction, current velocity, and wind speed. Beyond confirming the significant impact of waves on riser dynamics, it further reveals that the current velocity exerts a notable influence on riser bending moments. Moreover, a Monte Carlo-based probabilistic framework was employed to capture the joint uncertainties of all environmental parameters, which provides a more complete representation of environmental randomness than approaches that only consider single variables or a limited set of extreme conditions. With respect to riser safety, three key dynamic response parameters—the effective tension, bending moment, and von Mises stress—were examined. By combining probabilistic distribution fitting with reliability metrics, this study offers a more systematic perspective than methods focusing solely on maximum values. Finally, a global sensitivity analysis was applied to quantify the relative importance of environmental factors, providing a clear prioritization framework to support monitoring strategies and design optimization.

In summary, this study proposes a unified framework that integrates vessel–riser coupled modeling, environmental uncertainty representation, Monte Carlo simulation, a reliability analysis, and a sensitivity analysis. This framework enables both probabilistic failure assessments and quantitative sensitivity evaluations of key parameters. Building upon the reliability and sensitivity results, targeted monitoring priorities and safety strategies are recommended for different ocean environmental factors, offering direct applicability to riser design optimization and real-time operational monitoring.

Table 12. Comparison with previous research.

Studies	Methodology	Key Findings	Limitations
Wang et al. (2020) [10]	Numerical investigation of the dynamic behavior of deep-water pipelines during laying operations under the influence of vessel–riser coupling effects.	Without vessel–riser interaction, the wave load, wind, and current minimally affect the riser. Key factors influencing its dynamics are the wave height, spectral peak period, and direction.	Lack of risk probability modeling and quantitative assessment based on large-scale samples.
Wu et al. (2021) [13]	Numerical study of the dynamic response of the deep-sea mining vertical transport system (VTS) under irregular wave conditions considering vessel–riser interactions.	Wave-induced forces minimally affect the VTS equilibrium. Heave motion primarily determines the rigid riser tension, while the wave direction and height crucially influence VTS dynamics.	Lack of risk probability modeling and quantitative assessment based on large-scale samples; insufficient consideration of uncertainties in complex marine environments.
Chen et al. (2021) [12]	Development of a virtual prototype model for the deep-sea mining lifting system and experimental investigation of its dynamic response under various coordinated operations between the mining vessel and subsea mining equipment.	The nodal force at the connection between the submerged warehouse and pipeline increases with the mining ship heave amplitude, while bending moments mainly occur at the top and bottom of the pipeline.	Lack of risk probability modeling and quantitative assessment based on large-scale samples; insufficient consideration of uncertainties in complex marine environments.
Song et al. (2022) [11]	Numerical and experimental investigation of the dynamic behavior of vessel–riser coupled systems during deep-sea mining operations under regular wave conditions.	The riser constrains vessel motion. Vessel–riser coupling significantly affects the top tension and bottom displacement, with the interaction strongly influenced by the wave direction.	Lack of risk probability modeling and quantitative assessment based on large-scale samples; insufficient consideration of uncertainties in complex marine environments.
Hu et al. (2024) [21]	Development of a BP neural network model incorporating full-range ocean environmental parameters for predicting the dynamic response of the riser.	Predictive models enable rapid estimations of key riser dynamic responses.	Inadequate risk probability modeling and quantification; absence of a sensitivity analysis for ocean parameters.

4.2.2. Limitations and Applicability

While the proposed methodology demonstrates scientific and practical value, several limitations must be acknowledged.

To simplify the modeling framework, several assumptions were introduced in Section 2.1. Specifically, vessel elasticity, nonlinear wave–current interactions, friction, fatigue, material heterogeneity, and the complex interactions between pumps and intermediate buffer systems were neglected. Structural buckling and collapse were also not considered. Moreover, the model was developed for a representative 5000 m deep-sea mining scenario, and its applicability to other water depths, riser configurations, or vessel types requires further validation. The present method focuses primarily on short-term

extreme responses and failure probabilities, without explicitly accounting for long-term mechanisms such as vortex-induced vibration (VIV), cumulative fatigue, corrosion, or wear. In addition, the hydrodynamic coefficients used in this study were not fully validated against experimental data.

Future work should, therefore, aim to develop more refined contact mechanics and fluid–structure interaction models that incorporate vessel elasticity and material heterogeneity, enabling a more accurate description of vessel–riser coupling. The inclusion of VIV–fatigue interactions, hydrodynamic coefficient validation, and case studies across different depths and mining systems would further enhance the applicability of the method. Ultimately, extending the current framework to integrate probabilistic failure analyses with full life-cycle fatigue assessments, early-warning mechanisms, and a comprehensive risk management system will provide a more robust foundation for ensuring the safe operation of deep-sea mining risers.

There remains considerable potential to enhance the Monte Carlo simulation framework. For example, Hu et al. [21] employed a neural-network-based approach to efficiently train and validate large-scale sample datasets, which provides useful insights for the present study. To expand the sample size in Monte Carlo analyses while reducing the computational cost of vessel–riser coupled simulations, future work could integrate neural networks for uncertainty parameter modeling and surrogate response prediction. Such a hybrid approach would facilitate the generation of richer dynamic response datasets at substantially reduced computational cost, enabling more comprehensive probabilistic and sensitivity analyses.

5. Conclusions

In this study, a coupled vessel–riser dynamic model was established, integrating wave-induced vessel motions with hydrodynamic forces on the riser system. A frequency-domain hydrodynamic analysis using AQWA was employed to obtain the vessel RAOs, which were then incorporated into OrcaFlex for time-domain dynamic simulations. The effects of various oceanic environmental loads on the dynamic responses of the riser under vessel–riser coupling were systematically evaluated. Furthermore, a probabilistic risk analysis framework based on Monte Carlo simulations was constructed to assess the structural reliability of the riser and quantify the sensitivity of key uncertain environmental parameters on the system's dynamic response. Monte Carlo simulation offers distinct advantages in this study, enabling robust treatment of strong nonlinearities and multi-parameter couplings while interfacing with fully coupled vessel–riser numerical models. It provides direct access to the complete probability distributions of structural responses along with their associated confidence intervals and is fully compatible with Sobol-based global sensitivity analyses. Compared with traditional approaches such as AHP or fault tree methods, Monte Carlo simulation affords superior flexibility in representing arbitrary input distributions. The main conclusions are as follows:

(1) Under vessel-induced motions, the maximum effective tension of the riser occurs at the top connection with the vessel. Bending moments peak near the upper and lower sections of the riser, while network-based von Mises stress, primarily governed by axial tension, exhibits a trend similar to effective tension

(2) Significant wave height, wave period, and wave direction effects have notable impacts on the riser's effective tension, while the current speed has a relatively minor influence. The wind speed mainly affects riser dynamics indirectly via wave generation. Within the selected parameter ranges, the maximum deviations in effective tension were 1.42%, 1.06%, 9.27%, and 0.23%, respectively. The corresponding maximum variations

in bending moment were 3.36%, 5.74%, 26.57%, and 46.93%. For von Mises stress, the corresponding deviations were 1.43%, 1.06%, 9.72%, and 0.23%.

(3) Monte Carlo simulations were performed with 10,000 samples generated using Latin hypercube sampling based on realistic probability distributions of ocean environmental parameters. Results show that the riser could exceed allowable thresholds in terms of the effective tension and von Mises stress under extreme sea states, whereas bending moments would remain within safe limits.

(4) After applying a directional vector transformation to the wave direction, a sensitivity analysis using Spearman rank correlation revealed that significant wave height and wave period effects are the most dominant factors influencing the effective tension, bending moment, and von Mises stress. The sensitivity indices for these responses were approximately (0.785, 0.770, 0.074, 0.008, 0.013), (0.772, 0.759, 0.202, 0.005, 0.111), and (0.785, 0.770, 0.073, 0.008, 0.010), respectively. Additionally, wave directions aligned laterally (i.e., 90° or 270° relative to vessel heading) result in more pronounced structural responses. The current speed exhibited a uniquely higher influence on the bending moment due to its effect on the mid-span curvature of the slender riser.

From an engineering perspective, the integration of a vessel–riser coupled dynamic model with Monte Carlo simulation provides a valuable framework for the design, risk assessment, and operational monitoring of deep-sea mining risers. This study offers quantitative insights into the safe operating ranges of the effective tension, bending moment, and von Mises stress under uncertain ocean environmental conditions. The proposed risk probability analysis framework enables the evaluation of riser failure likelihood under varying sea states, which can be directly applied to inform safety margins. Furthermore, the sensitivity analysis results provide practical guidance for identifying the dominant environmental factors, allowing for the prioritization of targeted monitoring and operational safety strategies.

Author Contributions: Conceptualization, Q.H., G.W. and H.Z.; methodology, H.Z.; software, H.Z.; validation, G.W., H.Z. and Q.H.; formal analysis, H.Z.; investigation, H.Z., G.W. and Q.H.; resources, Q.H. and G.W.; data curation, H.Z. and Q.H.; writing—original draft preparation, H.Z.; writing—review and editing, Q.H. and G.W.; visualization, H.Z.; supervision, Q.H. and G.W.; project administration, Q.H. and G.W.; funding acquisition, Q.H. All authors have read and agreed to the published version of the manuscript.

Funding: This research was funded by the National Key Research and Development Project of China (2023YFC2811300).

Data Availability Statement: The original contributions presented in this study are included in the article. Further inquiries can be directed to the corresponding author.

Acknowledgments: The authors would like to thank the anonymous reviewers and editor for their constructive suggestions, which comprehensively improved the quality of the paper. All individuals have consented to the acknowledgement.

Conflicts of Interest: The authors declare no conflicts of interest.

References

1. Watzel, R.; Rühlemann, C.; Vink, A. Mining mineral resources from the seabed: Opportunities and challenges. *Mar. Pol.* **2020**, *114*, 103828. [CrossRef]
2. Petersen, S.; Krätschell, A.; Augustin, N.; Jamieson, J.; Hein, J.R.; Hannington, M.D. News from the seabed–Geological characteristics and resource potential of deep-sea mineral resources. *Mar. Pol.* **2016**, *70*, 175–187. [CrossRef]
3. Miller, K.A.; Thompson, K.F.; Johnston, P.; Santillo, D. An overview of seabed mining including the current state of development, environmental impacts, and knowledge gaps. *Front. Mar. Sci.* **2018**, *4*, 418. [CrossRef]

4. Ma, W.; Schott, D.; Lodewijks, G. Continuous Line Bucket Lifting Versus Pipe Lifting. *J. Offshore Mech. Arct. Eng.* **2017**, *139*, 051704. [CrossRef]
5. Kang, Y.; Wang, K.; Hu, Q.; Liu, S. Research on a coupled system design for mineral lifting and wastewater drainage in deep-sea mining applications. *Ocean Eng.* **2024**, *299*, 117260. [CrossRef]
6. Kang, Y.; Liu, S. The development history and latest progress of deep-sea polymetallic nodule mining technology. *Minerals* **2021**, *11*, 1132. [CrossRef]
7. Hu, Q.; Li, Z.; Zhai, X.; Zheng, H. Development of Hydraulic Lifting System of Deep-Sea Mineral Resources. *Minerals* **2022**, *12*, 1319. [CrossRef]
8. Wang, G.; Zhou, H.S.; Hu, Q. Failure detection for deep-sea mining lifting systems based on a hybrid LSTM-RF model. *Ocean Eng.* **2025**, *335*, 121772. [CrossRef]
9. Du, K.; Xi, W.; Huang, S.; Zhou, J. Deep-sea Mineral Resource Mining: A Historical Review, Developmental Progress, and Insights. *Min. Metall. Explor.* **2024**, *41*, 173–192. [CrossRef]
10. Wang, L.; Ju, M.; Xing, X.; Yun, F.; Wang, X. Dynamic Behavior of the Deepwater Flexible Pipeline during Pipe Laying Process. *J. Mar. Sci. Eng.* **2020**, *8*, 286. [CrossRef]
11. Song, Q.H.; Jiang, H.Y.; Song, Q.J.; Xiao, L.J.; Wang, Y. Study on vessel-pipe coupling dynamic behavior under regular waves in deep sea mining process. *Ocean Eng.* **2022**, *244*, 110401. [CrossRef]
12. Chen, W.; Xu, H.-L.; Peng, N.; Yang, F.-Q.; Lin, P. Linkage characteristics of deep-sea mining lifting system. *Ocean Eng.* **2021**, *233*, 109074. [CrossRef]
13. Wu, Q.; Yang, J.; Guo, X.; Liu, L. Influence of irregular waves on the dynamic response of a vertical transport system for deep sea mining. *Ocean Eng.* **2021**, *229*, 108443. [CrossRef]
14. Zhu, X.; Sun, L.; Li, B. Dynamic analysis of vessel/riser/equipment system for deep-sea mining with RBF neural network approximations. *Mar. Geores. Geotechnol.* **2020**, *38*, 174–192. [CrossRef]
15. Li, X.; Wei, W.; Bai, F. A full three-dimensional vortex-induced vibration prediction model for top-tensioned risers based on vector form intrinsic finite element method. *Ocean Eng.* **2020**, *218*, 108140. [CrossRef]
16. Sun, L.; Zhu, X.; Li, B.; Ai, S. Coupled dynamic analysis of deep-sea mining support vessel with dynamic positioning. *Mar. Geores. Geotechnol.* **2018**, *36*, 841–852. [CrossRef]
17. Adamiec-Wójcik, I.; Brzozowska, L.; Drąg, Ł. An analysis of dynamics of risers during vessel motion by means of the rigid finite element method. *Ocean Eng.* **2015**, *106*, 102–114. [CrossRef]
18. Chen, W.M.; Li, M.; Guo, S.X.; Gan, K. Dynamic analysis of coupling between floating top-end heave and riser's vortex-induced vibration by using finite element simulations. *Appl. Ocean Res.* **2014**, *48*, 1–9. [CrossRef]
19. Zhang, B.; Chai, Y.; Li, F.; Chen, Y. Three-dimensional nonlinear vortex-induced vibrations of top-tension risers considering platform motion. *Ocean Eng.* **2022**, *263*, 112393. [CrossRef]
20. Sun, H.; Feng, A.; You, Y.; Chen, K. Influence of the internal solitary waves on the deep sea mining system. *Ocean Eng.* **2022**, *266*, 113047. [CrossRef]
21. Hu, Q.; Qin, Y.; Zhu, J.; Zheng, M.; Huang, J.; Ou, Y. Research on Predicting the Mechanical Characteristics of Deep-Sea Mining Transportation Pipelines. *Appl. Sci.* **2024**, *14*, 7349. [CrossRef]
22. Cao, Y.; Gu, H.; Guo, H.; Li, X. Modeling and dynamic analysis of integral vertical transport system for deep-sea mining in three-dimensional space. *Ocean Eng.* **2023**, *271*, 113749. [CrossRef]
23. Xiao, J.; Kang, Z.; Chen, M.; Shen, Y.; Du, Y.; Leng, J. Dynamic Response Analyses and Experimental Research into Deep-Sea Mining Systems Based on Flexible Risers. *J. Mar. Sci. Appl.* **2024**, *24*, 789–804. [CrossRef]
24. Liu, Q.; Xiao, L. Analysis and Research on Longitudinal Vibration Characteristics of Deep Sea Mining Pipe Based on Finite Element Method. *Math. Probl. Eng.* **2020**, *2020*, 8219794. [CrossRef]
25. Huang, B.; Chen, J.; Liu, C.; Wang, L.; Wang, P. Analysis of vibration characteristics of lifting rigid pipe in deep-sea mining under ship movement. *Mar. Geores. Geotechnol.* **2025**, *43*, 356–370. [CrossRef]
26. Liu, J.; Zeng, L.; Guo, X.; Wang, P.; Dai, L. Multi-field coupling nonlinear vibration characteristics of hydraulic lifting pipe in deep-ocean mining. *Appl. Ocean Res.* **2022**, *120*, 103074. [CrossRef]
27. Li, Y.; Zhou, X.; Dou, Y.; Cao, H.; Li, W. Numerical analysis of parametric excitation characteristics of a deep-sea mining riser under vessel heave motions. *Ocean Eng.* **2025**, *328*, 121092. [CrossRef]
28. Jin, G.; Zong, Z.; Sun, Z.; Zou, L.; Wang, H. Numerical analysis of vortex-induced vibration on a flexible cantilever riser for deep-sea mining system. *Mar. Struct.* **2023**, *87*, 103334. [CrossRef]
29. Thorsen, M.J.; Challabotla, N.R.; Sævik, S.; Nydal, O.J. A numerical study on vortex-induced vibrations and the effect of slurry density variations on fatigue of ocean mining risers. *Ocean Eng.* **2019**, *174*, 1–13. [CrossRef]
30. Li, X.; Li, G.; Li, F.; Jiang, Y.; Gu, H. Numerical study on two-way coupled vortex-induced vibration of the lifting rigid pipe in deep-sea mining. *Mar. Geores. Geotechnol.* **2025**. [CrossRef]

31. Lin, T.; Bao, X.; Zhou, X.; Zuo, J.; Mou, Y. Study on vortex-induced vibration of non-uniform flow riser based on fluid-solid coupling. *IOP Conf. Ser. Earth Environ. Sci.* **2020**, *446*, 052039. [CrossRef]
32. Wang, Z.; Zou, L. Natural frequency analysis of deep-sea mining riser considering varying tension and buffer station. *Ocean Eng.* **2022**, *264*, 112372. [CrossRef]
33. Deng, L.; Lu, H.; Yang, J.; Guo, R.; Zhang, B.; Sun, P. Vortex-Induced Vibration of Deep-Sea Mining Riser Under Different Currents and Tension Conditions Using Wake Oscillator Model. *J. Mar. Sci. Eng.* **2025**, *13*, 1565. [CrossRef]
34. Dai, Y.; Li, X.; Yin, W.; Huang, Z.; Xie, Y. Dynamics analysis of deep-sea mining pipeline system considering both internal and external flow. *Mar. Geores. Geotechnol.* **2021**, *39*, 408–418. [CrossRef]
35. Duan, J.; Zhou, J.; You, Y.; Wang, X. Time-domain analysis of vortex-induced vibration of a flexible mining riser transporting flow with various velocities and densities. *Ocean Eng.* **2021**, *220*, 108427. [CrossRef]
36. Wang, R.; Chen, G.; Liu, X.; Zhang, N.; Liu, W. Safety analysis of deep-sea mining pipeline deployment operations considering internal solitary waves. *Mar. Geores. Geotechnol.* **2022**, *40*, 125–138. [CrossRef]
37. Gu, H.; Guo, H.; Bai, F.; Li, X.; Li, F. Study on the collision probability of vertical risers considering the wake interference effect. *Ocean Eng.* **2022**, *245*, 110583. [CrossRef]
38. Mao, L.; Yan, J.; Zeng, S.; Cai, M. Vortex-induced vibration characteristics of mining riser under the coupling effect of external ocean current and internal multiphase flow. *Appl. Ocean Res.* **2023**, *140*, 103747. [CrossRef]
39. Lavasani, S.M.; Ramzali, N.; Sabzalipour, F.; Akyuz, E. Utilisation of Fuzzy Fault Tree Analysis (FFTA) for quantified risk analysis of leakage in abandoned oil and natural-gas wells. *Ocean Eng.* **2015**, *108*, 729–737. [CrossRef]
40. Cheliyan, A.S.; Bhattacharyya, S.K. Fuzzy fault tree analysis of oil and gas leakage in subsea production systems. *J. Ocean Eng. Sci.* **2018**, *3*, 38–48. [CrossRef]
41. Wang, W.; Shen, K.; Wang, B.; Dong, C.; Khan, F.; Wang, Q. Failure probability analysis of the urban buried gas pipelines using Bayesian networks. *Process Saf. Environ. Prot.* **2017**, *111*, 678–686. [CrossRef]
42. Zhang, P.; Qin, G.; Wang, Y. Risk Assessment System for Oil and Gas Pipelines Laid in One Ditch Based on Quantitative Risk Analysis. *Energies* **2019**, *12*, 981. [CrossRef]
43. Ma, X.; Wang, Y.; Yang, K.; Li, J.; Li, Y.; Zhang, D.; Wang, R.; Fang, Y. Risk Assessment of International Seabed Mining Implementing the Analytic Hierarchy Process. *J. Mar. Sci. Eng.* **2025**, *13*, 937. [CrossRef]
44. Lu, C.; Yang, J.; Leira, B.J.; Skjetne, R.; Mao, J.; Chen, Q.; Xu, W. High-traversability and efficient path optimization for deep-sea mining vehicles considering complex seabed environmental factors. *Ocean Eng.* **2024**, *313*, 119500. [CrossRef]
45. Vanaei, H.R.; Eslami, A.; Egbewande, A. A review on pipeline corrosion, in-line inspection (ILI), and corrosion growth rate models. *Int. J. Press. Vessel. Pip.* **2017**, *149*, 43–54. [CrossRef]
46. Abyani, M.; Bahaari, M.R. A comparative reliability study of corroded pipelines based on Monte Carlo Simulation and Latin Hypercube Sampling methods. *Int. J. Press. Vessel. Pip.* **2020**, *181*, 104079. [CrossRef]
47. Atashgah, M.B.; Iranmanesh, M.; Mojtahedi, A. Investigation of a combined Monte Carlo simulation and Galerkin approach for probabilistic characteristics modelling the dynamic behaviour of the fluid-conveying pipe. *Ships Offshore Struct.* **2023**, *18*, 1594–1605. [CrossRef]
48. Li, A.; Jin, F.; Li, Y.; Lan, W.; Liu, P.; Yu, Z.; Wen, K. A Reliability Assessment Method for Natural Gas Pipelines with Corroded Defects That Considers Detection Cycles. *Energies* **2024**, *17*, 3366. [CrossRef]
49. Amaechi, C.V.; Wang, F.; Hou, X.; Ye, J. Strength of submarine hoses in Chinese-lantern configuration from hydrodynamic loads on CALM buoy. *Ocean Eng.* **2019**, *171*, 429–442. [CrossRef]
50. Biran, A.; López-Pulido, R. Numerical Integration in Naval Architecture. In *Ship Hydrostatics and Stability*, 2nd ed.; Biran, A., López-Pulido, R., Eds.; Butterworth-Heinemann: Oxford, UK, 2014; pp. 77–96. [CrossRef]
51. Shields, M.D.; Zhang, J. The generalization of Latin hypercube sampling. *Reliab. Eng. Syst. Saf.* **2016**, *148*, 96–108. [CrossRef]
52. *API RP 2RD-1998 (R2006)*; Design of Risers for Floating Production Systems (FPSs) and Tension-Leg Platforms (TLPs). American Petroleum Institute: Washington, DC, USA, 2006.

Disclaimer/Publisher's Note: The statements, opinions and data contained in all publications are solely those of the individual author(s) and contributor(s) and not of MDPI and/or the editor(s). MDPI and/or the editor(s) disclaim responsibility for any injury to people or property resulting from any ideas, methods, instructions or products referred to in the content.